Amphipathic helical peptides hamper protein-protein interactions of the intrinsically disordered chromatin nuclear protein 1 (NUPR1)

Patricia Santofimia-Castaño[a,1], Bruno Rizzuti[b], Olga Abián[c,d,e,f,g], Adrián Velázquez-Campoy[c,e,f,g,h], Juan L. Iovanna[a] and José L. Neira[c,i,1,*]

[a]*Centre de Recherche en Cancérologie de Marseille (CRCM), INSERM U1068, CNRS UMR 7258, Aix-Marseille Université and Institut Paoli-Calmettes, Parc Scientifique et Technologique de Luminy, Marseille, France;* [b]*CNR-NANOTEC, Licryl-UOS Cosenza and CEMIF.Cal, Department of Physics, University of Calabria, Rende, Italy;* [c]*Instituto de Biocomputación y Física de Sistemas Complejos, Joint Units IQFR-CSIC-BIFI, and GBsC-CSIC-BIFI, Universidad de Zaragoza, Spain*; [d]*Instituto Aragonés de Ciencias de la Salud (IACS), Zaragoza, Spain*; [e]*Aragon Institute for Health Research (IIS Aragon), Zaragoza, Spain*; [f]*Centro de Investigación Biomédica en Red en el Área Temática de Enfermedades Hepáticas y Digestivas (CIBERehd), Barcelona, Spain;* [g]*Departamento de Bioquímica y Biología Molecular y Celular, Universidad de Zaragoza, Zaragoza, Spain;* [h]*Fundación ARAID, Diputación General de Aragón, Zaragoza, Spain;* [i]*Instituto de Biología Molecular y Celular, Universidad Miguel Hernández, Elche (Alicante), Spain.*

[1] These two authors contributed equally to this work.

[*]Corresponding author address: José L. Neira, Instituto de Biología Molecular y Celular, Edificio Torregaitán, Universidad Miguel Hernández, Avda. del Ferrocarril s/n, 03202, Elche (Alicante), Spain. E-mail: jlneira@umh.es

Running title: Peptide binding to an IDP

Abbreviations: ANS, 8-anilino-1-naphtahlene sulfonic acid; CD, Circular dichroism; C-RING1B, C-terminal region of the Polycomb RING protein 1; IDP, intrinsically disordered protein; ITC, isothermal titration calorimetry; MD, molecular dynamics; MSL1, male specific lethal protein; NUPR1, nuclear protein 1; NMR, nuclear magnetic resonance; PDAC, pancreatic ductal adenocarcinoma; PLA, protein ligation assay; PPI, protein-protein interaction; SAM, sterile alpha motif; SLiM, short lineal motif; TFP, trifluoperazine.

ABSTRACT

Background: NUPR1 is a multifunctional intrinsically disordered protein (IDP) involved, among other functions, in chromatin remodelling, and development of pancreatic ductal adenocarcinoma (PDAC). It interacts with several biomolecules through hydrophobic patches around residues Ala33 and Thr68. The drug trifluoperazine (TFP), which hampers PDAC development in xenografted mice, also binds to those regions. Because of the large size of the hot-spot interface of NUPR1, small molecules could not be adequate to modulate its functions.

Methods: We explored how amphipathic helical-designed peptides were capable of interacting with wild-type NUPR1 and the Thr68Gln mutant, inhibiting the interaction with NUPR1 protein partners. We used *in vitro* biophysical techniques (fluorescence, circular dichroism (CD), nuclear magnetic resonance (NMR) and isothermal titration calorimetry (ITC)), *in silico* studies (docking and molecular dynamics (MD)), and *in cellulo* protein ligation assays (PLAs) to study the interaction.

Results: Peptide dissociation constants towards wild-type NUPR1 were ~ 3 μM, whereas no interaction was observed with the Thr68Gln mutant. Peptides interacted with wild-type NUPR1 residues around Ala33 and residues at the C terminus, as shown by NMR. The computational results clarified the main determinants of the interactions, providing a mechanism for the ligand-capture that explains why peptide binding was not observed for Thr68Gln mutant. Finally, the *in cellulo* assays indicated that two out of four peptides inhibited the interaction of NUPR1 with the C-terminal region of the Polycomb RING protein 1 (C-RING1B).

Conclusions: Designed peptides can be used as lead compounds to inhibit NUPR1 interactions.

General significance: Peptides may be exploited as drugs to target IDPs.

Keywords: Cancer, calorimetry, drug design, molecular dynamics, NMR, peptides.

1. INTRODUCTION

Protein-protein interactions (PPIs) are critical for molecular communications and processes such as cell division, transcription, signal transduction and programmed cell death. PPIs are also key in the development of various diseases and pathological conditions, such as neurodegeneration and cancer (1,2). PPIs can occur between two structured proteins (or domains); two IDPs; a well-folded protein and an IDP; a folded domain and a short peptide; or between two peptides (3). In those interactions, the secondary structural element α-helix appears in 62 % of all interfaces (4,5). Therefore, drugs inhibiting specific PPIs involving α-helices could have an important therapeutic potential. However, the use of small molecules targeting PPIs is difficult due to two reasons. First, interface regions in PPIs are usually large (700-3000 $Å^2$) (6), with many polar and hydrophobic interactions. And second, the interfaces are typically shallow, with lack of a clear pocket to allow binding of a small molecule (7). Thus, the chemical space of small molecules deviates from that of PPI inhibitors, perhaps explaining the low hit rates of small drugs in PPI inhibition (7,8). Peptides and peptidomimetics (i.e., modified peptides) can be used to target PPIs; in fact, 15-40 % of all possible PPIs involve a linear peptide (9,10). Peptides can have several advantages against small molecules in targeting a protein-protein interface; the most important one is that they can be rationally designed on the basis of the protein sequences of their binding partners. Peptidomimetics further combine the folding properties of peptides, with the lack of proteolytic and metabolic degradation (11,12). In a structure-based approach to drug-design, peptide binding regions derived from protein-protein interfaces can be used as a starting point for the design of PPI inhibitors. However, if the aim is to target an isolated IDP, which is basically an ensemble of rapidly inter-converting conformational states, the design of peptides or peptidomimetics capable of hampering its biomolecular interactions is even more challenging.

NUPR1 is an 82-residue-long (8 kDa), highly basic, monomeric IDP that is over-expressed during the acute phase of pancreatitis (13). It does not have a stable secondary and tertiary structure

in any region of its sequence, as occurs in most of other IDPs (14-16). NUPR1 is believed to function during transcription, and it is an essential element in the stress cell response and cell-cycle regulation, but its exact functions are not fully understood (17,18). It plays key roles in pancreatic tumorigenesis, acting downstream of the $Kras^{G12D}$ oncogene mutation, which is critical for pancreatic carcinogenesis (19). Furthermore, NUPR1 is involved in apoptosis by forming a complex with prothymosin α (20), another IDP, as well as implicated in DNA binding (21) and repair (22), through interaction with the male specific lethal protein (MSL1), and in the association to proteins of the Polycomb group (23). All these interactions provide the rationale to consider NUPR1 inhibition as a clinically feasible strategy to expand the PDAC drug arsenal.

We have shown that binding to all those biomolecules occurs through two distant regions of the NUPR1 sequence (20, 22-24): (i) the hydrophobic patch around Ala33, containing the two aromatic rings of the protein, Tyr30 and Tyr36; and, (ii) the region around Thr68, which is a polypeptide patch with relatively high hydrophobicity. The Ala33Gln and Thr68Gln mutants have both shown impaired binding to NUPR1 protein partners, therefore pinpointing the importance of those regions (23). As tested in PDAC-derived cell-based assays (24), both regions also intervene in the binding of small molecules capable of inducing cell-growth arrest and senescence, reduced cell migration, and decreased chemoresistance, thus mimicking NUPR1-deficiency. In fact, one of those drugs, TFP, completely abolishes tumor development *in vivo* on xenografted PDAC-derived cells in mice (24). Therefore, the same hot-spot NUPR1 regions involved in binding to its natural biomolecular partners are also implicated in the binding to small compounds with potential therapeutic action. Given the importance of α-helices in PPIs (4,5), in this work, we investigated the use of synthetic peptides, with an improved tendency to form amphipathic α-helices in solution, to target the same hydrophobic hot-spot regions of NUPR1, and acting as inhibitors of the PPIs of NUPR1. Bioactive peptides of different origins have shown anti-cancer properties ((25) and references therein), and the possibility of using them in the treatment of tumors, targeting IDPs, is

intriguing. It is important to pinpoint that this is the first report of the design of peptides that can bind NUPR1. Therefore, we benchmarked the use of helical-designed peptides to target an IDP and hamper its protein-protein interactions, and we studied the peptide effects against NUPR1 *in vitro*, *in silico*, and *in cellulo*.

To test this hypothesis, we carried out an *in vitro* characterization of the binding between a series of peptides derived from the wild-type sequence Ac-VKNWMTETLLVQ-NH_2. This sequence, which was originally obtained from the capsid protein of HIV-1, is highly amphipathic, having an intrinsic tendency to adopt helical conformations and to self-associate (26). Three other peptides have been designed *in silico* to have a better helicity than the wild-type sequence (27,28), without altering their amphipathic features (26). The four peptides were assayed through spectroscopic (namely, fluorescence, CD and NMR) and calorimetric (ITC) techniques against NUPR1. In addition, *in silico* studies were carried out to reveal the key determinants in their binding to NUPR1. Finally, *in cellulo* assays were carried out by means of PLAs. Our hypothesis-driven experiments showed that there was binding between wild-type NUPR1 and the helical-designed peptides both *in vitro* and *in cellulo*, with a dissociation constant of ~ 3 μM. The peptide binding region of NUPR1, as mapped by NMR spectra, involved: (i) the hydrophobic patch at the 30s region of the protein; and, (ii) other residues located at both protein termini. The ITC control experiments with the NUPR1 Thr68Gln mutant further suggested that this residue was important for peptide binding. Blind *in silico* studies showed that binding occurred through the same NUPR1 hot-spot region detected in the NMR studies, providing an anchoring to a specific region of the peptide surface, and suggesting a rationale for the experimental lack of binding of the Thr68Gln mutant. The PLAs indicated that the interactions of wild-type NUPR1 with C-RING1B were completely abolished *in cellulo* in the presence of two out of the four peptides; the activity of the other two could not be assessed, likely due to cytotoxicity or peptide inability to penetrate the cells. Our findings suggest that NUPR1 interactions with its natural partners can be hampered by the use of designed amphipathic α-helical

peptides, based exclusively on physico-chemical grounds (amphipathy and helicity). Moreover, our results represent a proof-of-concept that peptides can be rationally designed against IDPs to inhibit their PPIs.

2. MATERIALS AND METHODS

2.1. Materials

Deuterium oxide was obtained from Apollo Scientific (UK). Sodium trimethylsilyl [2,2,3,3-$^{2}H_4$] propionate (TSP), imidazole, Trizma base, ANS, deuterated acetic acid and its sodium salt, and nickel resin were from Sigma-Aldrich (Spain). Dialysis tubing, with a molecular weight cut-off of 3500 Da, was from Spectrapor (Spectrum Laboratories, Japan). Amicon centrifugal devices with a cut-off molecular weight of 3000 Da were from Millipore. Standard suppliers were used for all other chemicals. Water was deionized and purified on a Millipore system.

2.2. Proteins expression and purification

Wild-type NUPR1 and the Thr68Gln mutant were produced and purified in Luria-Bertani (LB) media as described (21-23) in C41 cells (29). For ^{15}N-labelled wild-type NUPR1 the same cell growth protocol as in LB was used, with $^{15}NH_4Cl$ (1 gr per litre of media) as the sole source of nitrogen, with M9 medium, a vitamin mix and a mixture of metal ions to improve bacterial growth. The yield of the protein in such minimal medium was roughly 2/3 of that obtained in LB. After purification (either from LB or in minimal media), the protein was extensively dialyzed against water. Given the poor expression of the Thr68Gln mutant in rich media (23), we did not attempt to label it. The mutation at the other hot-spot region of NUPR1, Ala33Gln, resulted in lack of protein expression (23). Protein concentration was determined from the absorbance of the two tyrosines in the amino acid sequence (30).

2.3. Design and synthesis of the peptides

Our initial design for the peptide sequence was Ac-VKNWMTETLLVQ-NH_2. This peptide is a part of the capsid protein of HIV-1 (residues Val181-Gln192 of the whole sequence); in the intact protein, this patch forms an α-helix through which the capsid protein dimerizes (31,32). The predicted percentage of helical structure for this peptide, according to AGADIR (27,28), was 4.6 %, and that obtained experimentally from CD measurements was 6.9 % (26). All the peptides had a

tendency to self-associate with dimerization constants in the order of 4 μM (26). The other three peptides (Table 1) were designed, by using AGADIR, with the aim to improve the helicity of the wild-type peptide. The increase of the predicted helicity in the designed peptides was probably due to stabilization through a stacking interaction between the two aromatic rings of the natural Trp4 and the mutated Tyr8 (located on the same side of the helix), and a capping effect at the C terminus of the helix. The experimentally determined helicity was always lower than that predicted. Peptide concentrations were determined from the absorbance of aromatic residues (30).

All the peptides were synthesized by GenScript (New Jersey, USA) with a purity larger than 95 %, as tested by chromatography and mass spectrometry.

2.4. Fluorescence

Fluorescence spectra were collected on a Cary Varian spectrofluorimeter (Agilent, USA), interfaced with a Peltier, at 25 ºC. Experiments were carried out at pH 6.8 (20 mM phosphate buffer). The samples were prepared the day before and left overnight at 5 ºC. Before experiments samples were left for 1 h at 25 ºC. NUPR1 concentration (either wild-type or Thr68Gln mutant) was 15 μM, and the corresponding peptide concentration was 20 μM (in protomer units). For experiments in the presence of ANS, a final concentration of 100 μM of the probe was added; peptide and protein concentrations were the same as in the experiments where the intrinsic fluorescence was monitored. A 1-cm-pathlength quartz cell (Hellma) was used.

(a) Steady-state spectra (intrinsic and ANS)- To follow the intrinsic fluorescence of tyrosine and/or tryptophan, samples were excited both at 280 and 295. The slit widths were 5 nm for both the excitation and emission lights. The spectra were recorded between 300 and 400 nm. The signal was acquired for 1 s and the increment of wavelength was set to 1 nm. Blank corrections were made in all spectra.

The same experimental set-up was used for experiments in the presence of ANS, but the excitation wavelength was 370 nm and emission light was collected from 400 to 600 nm. Only experiments with the wild-type NUPR1 were carried out with this probe.

(b) Thermal denaturations- Thermal denaturations were carried out in samples containing ANS and wild-type NUPR1, by following the fluorescence at 480 nm, after excitation at 370 nm. The scan rate was 60 ºC/h, data were collected every 0.2 ºC and the average time was 1 s.

(c) Binding experiments- For the titration between the peptides and wild-type NUPR1, increasing amounts of NUPR1, in the range 0-10 μM, were added to a solution with a fixed concentration of the corresponding peptide (2 μM, in protomer units). The experimental set-up was that described above, except that excitation wavelength was only 295 nm (to avoid subtraction of the increasing amount of NUPR1 used during the titration); in that way, we were only monitoring the Trp4 of the peptides during the experiment. The experiments were acquired at 25 ºC in phosphate buffer, 50 mM (pH 7.4). The samples were prepared the day before and left overnight at 5 ºC; before measurements, the samples were incubated 1 hour at 25 ºC. The fluorescence values of a blank solution containing only the corresponding peptide were subtracted for each point. The dissociation constant of the peptide/NUPR1 complex, K_D, was calculated by fitting the plot of the observed fluorescence change of Trp4 *versus* added NUPR1 to (33,34):

$$F = F_0 + \frac{\Delta F_{max}}{2[P-i]_T}\left[\left([P-i]_T + [\mathrm{NUPR1}]_T + K_d\right) - \left(\begin{matrix}\left([P-i]_T + [\mathrm{NUPR1}]_T + K_d\right)^2 - \\ 4[P-i]_T[\mathrm{NUPR1}]_T\end{matrix}\right)^{1/2}\right] \quad (1),$$

where F is the measured fluorescence at any particular concentration of NUPR1 after subtraction of the blank; ΔF_{max} is the maximal change in the fluorescence of the P-i peptide when all of NUPR1 is forming the complex compared to the fluorescence of isolated P-i peptide; F_0 is the fluorescence intensity when no NUPR1 was added; $[P\text{-}i]_T$ is the constant, total concentration of the corresponding peptide (2 μM, in protomer units); and $[NUPR1]_T$ is that of NUPR1, which is varied during the titration. The titration with each peptide was repeated twice. At all used concentrations, the

absorbance of NUPR1 was kept lower than 0.2 units of absorbance (at 280 nm) to avoid inner-filter effects, during fluorescence excitation (35).

2.5. CD spectroscopy

CD spectra were collected on a Jasco J815 spectropolarimeter (Jasco, Japan) fitted with a thermostated cell holder, and interfaced with a Peltier unit. The instrument was periodically calibrated with (+) 10-camphorsulphonic acid. The wild-type NUPR1 and the peptide concentrations were 15 μM and 20 μM (in protomer units), respectively for the experiments of complex formation.

(a) Steady-state spectra: Experiments were acquired at pH 6.8 (20 mM phosphate buffer) with a scan speed of 50 nm/min, a response time of 2 s, a band width of 1 nm, and averaged over six scans at 25 ºC. All spectra were corrected by subtracting the corresponding baseline. Samples were prepared the day before and left overnight at 5 ºC.

(b) Thermal denaturations- Thermal denaturations were carried out with a band width of 1 nm, a response of 8 s and a scan rate of 60 ºC/h. Data were collected every 0.2 ºC, following the raw ellipticity at 222 nm.

2.6. NMR spectroscopy

The NMR experiments were acquired on a Bruker Avance DRX-500 spectrometer equipped with a triple resonance probe and *z*-pulse field gradients. Experiments were acquired at 25 ºC and pH 4.5 (acetate buffer, 50 mM), by adding the corresponding amount (50 μL) of a stock solution of 0.5 M deuterated acid in D_2O; probe temperature was calibrated with a methanol NMR standard (36). We carried out the experiments at that pH to allow for the detection of the largest possible number of cross-peaks, since at pH 7.0 only 10 residues are observed (23). The pH of the samples was measured before and after the experiments with an ultra-thin electrode (Sigma-Aldrich); for all the peptides during the titrations the pH at both measurements was 4.5 ± 0.2.

The peaks in the 2D $^{1}H,^{15}N$-HSQC (37) NMR spectra of NUPR1 were identified by using previously determined assignments at pH 4.5 (22). The HSQC was acquired by using sensitivity

enhancement with echo-antiecho-TPPI and gradient selection (36), with the carrier proton frequency at 8.00 ppm, and a spectral width in the ^{1}H dimension of 6.00 ppm. With this spectral width and the phase cycling used in the corresponding sequence from the Bruker library (hsqcetgp) the water signal was not observed. A concentration of wild-type ^{15}N-labelled NUPR1 of 190 μM was used, and the corresponding amount of peptide (in the concentration range from 200 to 400 μM, in protomer units) was added. Experiments to determine which residues were first affected upon addition of the corresponding peptide were carried out at specific peptide concentrations (indicated in Table 2). 2D ^{1}H,^{15}N-HSQC spectra were also acquired at 115 μM of NUPR1 with increasing concentrations of each of the peptides in the range 7 to 50 μM (in protomer units). In this case, the spectra were acquired with the TPPI method (36) with the carrier proton frequency at the water frequency, which was removed by presaturation. In these titration experiments, a fresh sample of ^{15}N-labelled NUPR1 was prepared for each peptide concentration.

The spectra at each particular peptide concentration were typically acquired with 2 K complex points in the ^{1}H dimension, 128 (or 200 for the titration experiments) complex points in the ^{15}N dimension, with 64 scans per increment (or 128 scans for the titration experiments). Typical spectral widths for all experiments were 6000 (^{1}H) and 1500 (^{15}N) Hz. The resulting matrix of each experiment was zero-filled to double the number of original points in each dimension and shifted squared sine-bell apodization functions were applied, prior to Fourier transformation. NMR data were processed and analyzed using TopSpin 2.1 (Bruker). Signal intensities in the NMR experiments in the presence of a fixed amount of the peptides were measured by using the same program, by comparison with the cross-peak intensity of the C-terminal residue, Arg82. For the titration experiments, intensities were reported as absolute values, after correction for the receiver gain value. Spectra were referenced with external TSP for ^{1}H, and for the indirect dimension as described (36).

2.7. ITC

Peptide binding to either wild-type NUPR1 or Thr68Gln mutant was determined with a high sensitivity isothermal titration calorimeter Auto-iTC200 (MicroCal-Malvern Instruments, Malvern UK), with reference power of 10 μcal/s, initial delay of 60 s, spacing between injections of 150 s. Protein and peptide concentrations were estimated by using their theoretical absorption extinction coefficients (30).

Protein samples and reference solutions were properly degassed to avoid bubble formation during stirring. Experiments were performed with freshly prepared protein solutions, at 15 °C in 50 mM Tris pH 7.4, with 2 % DMSO, to improve peptide solubility. A 20 μM solution of either wild-type or Thr68Gln NUPR1 was titrated into the calorimetric cell with 300-400 μM peptide solution from the injecting syringe. NUPR1 did not show any evidence of aggregation at these concentrations used (nor, at least, up to a concentration of 2 mM, where protein assignment was carried out (22)). A sequence of 19 injections of 2 μL volume was programmed with a stirring speed of 750 rpm. The heat evolved after each ligand injection was obtained from the integral of the calorimetric signal. Control experiments (peptide injected into buffer) were performed under the same experimental conditions. The association constant (K_a) and the enthalpy change (ΔH) of the binding reaction were obtained through non-linear regression of experimental data to a model for a protein with a single ligand binding site. Experiments were performed in replicates and data were analyzed using in-house developed software implemented in Origin 7 (OriginLab, Northampton, MA). We analyzed the titrations including a parameter accounting for the background injection heat effects (which are not much larger than the heat effect due to the interaction), and, therefore, we estimated the dissociation constants and the binding enthalpies with sufficient reliability. The background injection heat effects represent the reference heat in the absence of the interaction along the titration; therefore, the departure from that reference value (in our case, upward or endothermically), whatever the value of the background injection heat effect, reflects the heat effect due to the molecular interaction. Blanks

or controls injecting titrant into buffer were performed in order to rule out any potential artifacts or the possible effect from titrant self-dissociation.

2.8. Molecular modeling and dynamics

The structures of the peptides, including the capping at their termini, were built by using the chemical editors Avogadro (38) and VMD (39). The complete structure of each peptide was refined through MD simulations in water, to obtain a representative ensemble of eight different conformations. The simulation package GROMACS (40) was used in combination with the AMBER ff99SB-ILDN force field (41) and the TIP3P water model (42). For the two charged peptides, P-1 and P-3, a chloride counterion was added to obtain an overall neutral system. The peptides were first equilibrated for 1 ns, and then a production run was carried out for other 2 ns at room temperature and pressure. Simulation conditions, including reference values and coupling times for the thermostat and barostat, modeling of the electrostatics and van der Waals interactions, as well as treatment of atomic distance constraints and periodic boundary conditions, were as described (43,44).

An ensemble of structures of NUPR1, either from wild-type or Thr68Gln mutant, was obtained following a protocol previously reported for IDPs (45, 46), with the protein structure initially built in extended conformation and then collapsed in a long-term run (40 ns) performed in the presence of explicit water molecules. Simulation of peptide/NUPR1 complexes were built starting from unbound NUPR1 with equilibrated gyration radius (2.2 nm), as it was experimentally measured (24). To assess potential artifacts due to overcompaction of the IDP structure, additional control simulations were performed using the TIP4P-D water model (47) which is specifically suited to address such deficiency. Water topology was built in the required GROMACS format by using as a starting model the one of TIP4P/2005 (48) which shares the same geometry, and modifying charges and Lennard-Jones parameters as required (47).

2.9. Molecular docking

The binding affinity of NUPR1 and each peptide was evaluated by performing a systematic molecular docking. Portions of the NUPR1 sequence containing seven consecutive protein residues were considered, with the rest of the backbone truncated and capped when necessary (by using an acetyl and amide group at the N and C terminus, respectively). The graphical interface AutoDock Tools 1.5.6 (49) was used to prepare the system, and molecular docking was performed by using AutoDock Vina (50) at high exhaustiveness (eight times larger than the default value).

2.10. PLA

HeLa cells were seeded in 12-well plates on coverslips and transfected with 2 µg of DNA (NUPR1-FLAG and RING1B-HA) and 2 µL of Lipofectamine 3000 Transfection Reagent (Thermo Fisher Scientific) per well. Cells were assayed after 28 h post-transfection. To transport the peptides or FITC-antibody (as control) into HeLa-transfected cells, Pro-JECT^{TM} Protein Transfection Reagent Kit (Thermo Fisher Scientific) was used following manufacturer's recommendations. Briefly, peptide solution (in DMSO) was added to a tube containing a dry film of Pro-JECT reagent and incubated for 5 minutes. Then, Opti-MEM medium was added to bring the final delivery volume to 500 µL. Finally, regular culture media was aspirated from the wells and the delivery mix was transferred to the cells. The cells were incubated for 4 h. After that, cells were washed twice in phosphate buffer solution (PBS), fixed, washed twice again, permeabilized in PBS/0.1% Triton X-100 and saturated with Blocking Solution for 30 min before immune-staining with Duolink® by using PLA® Technology (Sigma-Aldrich) following the manufacturer's protocol. Slides were processed for *in situ* PLA by using sequentially the Duolink® In Situ Detection Reagents Red, Duolink® In Situ PLA® Probe Anti-Mouse MINUS, and Duolink® In Situ PLA® Probe Anti-Rabbit PLUS. The following antibodies were used: mouse monoclonal anti-HA (12CA5, Santa Cruz Biotechnology) and rabbit anti-human NUPR1 antibody chemically synthesized (Neosystem, France) following previously described methods (22,23). In these experiments, monitored red fluorescence corresponds to the PLA positive signal, and it indicates that the two molecules belong to the same

protein complex. Blue fluorescence corresponds to nuclei (the so-called DAPI staining). To check the specificity of the PLA signal, negative control experiments omitting one of the primary antibodies were performed. Unspecific binding was optimized by using the proper antibodies and optimizing the transfection times. Protein over-expression during the experiments was used to obtain a clearer and better signal.

Preparations were mounted using Prolong Gold antifade reagent (Invitrogen) and image acquisition was carried out on a Nikon Eclipse 90i fluorescence microscope.

3. RESULTS

3.1. The design of the peptides

Our initial wild-type sequence for the peptide was Ac-VKNWMTETLLVQ-NH_2. This peptide was derived from the all-α-helical wild-type capsid protein of HIV-1 (residues Val181-Gln192 of the whole sequence) (Table 1); the peptide sequence is highly amphipathic, and it self-associates to favour contact among the different subunits in the viral capsid. Therefore, it could be a good lead peptide to test amphipathy and helicity in the design of peptides capable of targeting NUPR1. The original sequence (hereafter, named P-4) was modified by using AGADIR software (27,28) to improve its helicity; the rationale behind the chosen substitutions of residues has been described previously, and it is briefly described in section 2.3. (26). Experimental measurements on the three derived peptides (the two single mutants P-1 and P-2, and the double mutant P-3), performed by using far-UV CD and measurements of the ellipticity at 222 nm and titration in the presence of organic co-solvents, revealed that the helicity value was lower than that theoretically predicted (26) (Table 1); probably the peptides are populating in aqueous solution several conformations involving helix- or turn-like structures. The peptides have also a self-association tendency with affinities in the order of ~4 μM (26). This tendency precluded their NMR characterization in aqueous solution.

3.2. The peptides interacted with wild-type NUPR1 in vitro

To test whether the peptides and wild-type NUPR1 interacted *in vitro* we followed a three-part approach. As a control, we used the mutant Thr68Gln, which does not show binding to some of the protein partners of NUPR1 (23). First, we tried fluorescence experiments with the four peptides and with wild-type NUPR1 and the Thr68Gln mutant either by acquiring steady-state spectra (in the absence and in the presence of 8-anilino-1-naphtahlene sulfonic acid (ANS)) or by acquiring thermal denaturations of the complexes. We used the steady-state fluorescence spectra to determine whether there were rearrangements in the binding pocket occupied by ANS or, alternatively, in the neighborhood of the sole Trp in the peptides, upon binding of the two biomolecules (NUPR1 only

has two tyrosine residues). The use of ANS to monitor binding deserves an explanation, because it usually binds to hydrophobic patches in proteins. That is why, usually, ANS shows low binding (and small fluorescence emission) to a folded protein, and high binding (and large fluorescence emission) to an unfolded one; therefore, it can be used as an extrinsic fluorescent probe to monitor protein unfolding. However, ANS does not always follow that behavior: there are some proteins displaying higher ANS binding (or, at least, larger fluorescence emission) when they have a larger amount of structure, such as prothymosin α, nucleobindin (Calcnuc) and Tim15 (51-53). From our experience, we have also observed ANS binding to IDPs. For example, NS3 protease from hepatitis C virus is partially unstructured in the absence of its zinc metal cofactor; this protein binds ANS when partially unstructured, and then increases ANS binding as it unfolds completely along a temperature denaturation (54-56). The same behavior was observed in NUPR1 when it is bound to small drugs (24). On the other hand, we have also observed that ANS (and other fluorescent probes) sometimes does not work as an extrinsic probe with some folded proteins, contrary to the usual expectation.

Our results show that, when both peptide and NUPR1 were present together in solution, the environment around ANS (Fig. 1 A) and that around Trp4 (Fig. 1 B) of the peptides changed (Fig. 1 shows, as a representative example, the data for P-3; data for the rest of the peptides are shown in Fig. S1). As it can be observed, NUPR1 showed variation in the amount of solvent-exposed hydrophobic regions in the presence of the peptides. Experiments with the Thr68Gln mutant and P-3 suggest the absence of binding (Fig. S2), following the intrinsic fluorescence of the protein, the peptide and the complex. The finding that there are differences between the spectrum of the intrinsic fluorescence of the complex formed and that obtained from the sum of the spectra of both isolated macromolecules suggests that the environment around Trp4 of the peptides, or that of the two tyrosines of NUPR1, are being affected by binding (Fig. 1 B). A similar conclusion can be drawn from the fluorescence spectrum of ANS: the environment around the probe (and thus solvent-exposed hydrophobic patches) changes in the presence of both molecules (Fig. 1 A).

In addition, we suspected that those protein-peptide interactions, detected by steady-state spectra of intrinsic fluorescence or ANS, may promote some limited, small structural rearrangements in wild-type NUPR1, resulting in a different fluorescence thermal-denaturation pattern compared to that of the unbound protein. To elucidate whether there were changes in the conformational ensemble of wild-type NUPR1 upon peptide binding, we carried out thermal denaturations in the presence of ANS, whose fluorescence changes seem to be larger than those of the intrinsic fluorescence of the peptide/NUPR1 complex; we did not carry out experiments with the peptides and Thr68Gln mutant with ANS because of the absence of binding (Fig. S2). Thermal denaturations in the presence of ANS followed a different pattern for isolated P-3, isolated wild-type NUPR1, and the P-3/NUPR1 complex (Fig. 1 C), but for none of the three solutions a sigmoidal behavior was observed in the unfolding traces. This different behavior for several polypeptide chains or complexes during thermal denaturations, monitored by ANS, has been observed in other proteins. As explained above, ANS (and other fluorescent probes) does not always follow the usual expected behavior when monitoring thermal denaturations of folded proteins by the extrinsic ANS fluorescence (57). From our experience, we have observed ANS binding to IDPs, such as NS3 protease from hepatitis C virus (see above). A similar tendency is observed in NUPR1 (24) when is bound to small drugs. Even if the protein is completely unfolded, it may show some weak ANS binding; on the other hand, the same protein when interacting with a molecule may show a different ANS binding. In addition, both free- and bound- protein may display a different unfolding profile monitored by ANS along the temperature denaturation. This observation can be employed for observing interaction between binding partners, as well as for identifying binding compounds in IDPs or well-folded proteins. Therefore, we could conclude from the fluorescence results that there were interactions between the peptides and wild-type NUPR1, and that these interactions were not present with the Thr68Gln mutant.

The fluorescence changes induced by the peptides in the wild-type NUPR1 spectrum are an indirect piece of evidence of the interaction, as variations in thermal denaturations and steady-state

spectra may be the result of unspecific interactions between the peptides and NUPR1. Then, at a second stage, we used ITC (58) to determine the dissociation constants, K_Ds, of the peptides for NUPR1. The K_Ds for the peptide/NUPR1 complexes were in the low micromolar range, indicating that the peptides bound specifically to NUPR1 and they would represent a good starting point for further affinity optimization to obtain binders with a higher specificity (Table 1, Fig. 2). We further used ITC to determine the importance of Thr68 on the binding properties of NUPR1. Since we have already observed that this mutation decreases the affinity of NUPR1 for C-RING1B (23), we decided to test by ITC whether the peptides were bound to Thr68Gln mutant. No binding was observed with the mutant protein for any of the peptides under the same conditions explored for wild-type NUPR1 (Fig. S3), and thus, we conclude that Thr68 is a key residue to achieve peptide association.

We also measured the K_D of the peptides by using fluorescence; in that experiment we were certain that upon binding to NUPR1 the environment around Trp4 in the peptides was modified upon binding to NUPR1. In all cases, the measured affinity constants were similar to those reported by ITC (Table 1, Fig. S4). These experiments confirm that the binding was specific and that it occurred around the sole tryptophan of the peptides.

As the peptides partially self-associate (26), if they were bound to NUPR1 in monomeric form, then the dimerization equilibrium of the peptide would be coupled to the binding equilibrium towards NUPR1. Because the binding to NUPR1 implies binding of the monomeric species or dissociation of the dimeric species of the peptide, then, the apparent dissociation constant for the peptide/NUPR1 interaction, K_D^{app}, will be larger than the intrinsic dissociation constant for the peptide/NUPR1 interaction, K_D (i.e., the dissociation constant if all peptide molecules are in monomeric form). In particular, the apparent dissociation constant for the peptide/NUPR1 interaction is given by:

$$K_D^{app} = K_D\left(1+\frac{2[L]}{K_{sD,pep}}\right) = K_D\left(1+\frac{2[L_2]}{[L]}\right),$$

where $K_{sD,pep}$ is the self-dissociation constant for the peptide monomer-dimer equilibrium ($K_{sD,pep}=[L]^2/[L_2]$). From the above expression, we can conclude that if the peptide self-association equilibrium is displaced towards the monomer ($K_{sD,pep}$ very high and $2[L_2]/[L]<<1$), then K_D^{app} is roughly equal to K_D (the observed affinity is similar to the intrinsic affinity for the monomeric peptide). However, if the peptide self-association equilibrium is displaced towards the dimer ($K_{sd,pep}$ very low and $2[L_2]/[L]>>1$), then K_D^{app} is much larger than K_D (i.e., the observed affinity is much lower than that of the monomeric peptide).

And at a third stage, we carried out far-UV CD experiments of the peptide/NUPR1 complexes. For all the peptides, there were no changes in the addition spectrum (obtained from the sum of those of the two isolated polypeptides) and that of the corresponding peptide/NUPR1 complex (Fig. S5 A), indicating that the conformational ensemble of the peptide and/or wild-type NUPR1 remained the same after binding. Furthermore, the absence of a sigmoidal behavior in the thermal denaturations (Fig. S5 B) suggests that wild-type NUPR1 remained disordered upon peptide binding.

To sum up, the three techniques (fluorescence, ITC and CD) showed that peptides and wild-type NUPR1 interacted *in vitro* with a low affinity constant in the range of 4 μM. This interaction was hampered in the Thr68Gln mutant.

3.3. The peptide binding mapped to a hydrophobic region located at the 30s of NUPR1 sequence

To characterize the molecular bases behind the formation of the peptide/NUPR1 complexes, we sought to determine the NUPR1 regions involved in binding. Since we have previously reported the NMR assignment of all residues of wild-type NUPR1 (22) (BMRB number 19364), we used 2D $^{1}H,^{15}N$-HSQC spectra of wild-type NUPR1 to monitor changes upon peptide addition.

At pH 4.5, upon addition of any of the peptides, the NUPR1 cross-peaks broadened (Fig. 3 shows as a representative example the data for P-2, whereas the rest of the HSQC spectra for the other peptides are shown in three panels in Fig. S6); the changes were larger in P-2 (Table 2), for which many of the NUPR1 resonances disappeared. It could be thought that the intrinsic self-association of P-2 could be responsible for this general broadening of most of NUPR1 cross-peaks;

however, the fact that the self-association constants for the four peptides is the same (~4 μM, (26)) and that the assayed concentration of the peptides was nearly the same (Table 2), suggest that there were other factors affecting peptide binding to NUPR1. In P-1, P-3 and P-4 peptides, only the relative intensity of several cross-peaks were affected, suggesting that the binding was specific (as further pinpointed by ITC and fluorescence). In general, the most affected regions of NUPR1 upon addition of any of the four peptides were: (i) around Ala33, where the two aromatic residues of NUPR1 are located (Tyr30 and Tyr36); and, (ii) the C-terminal region (close to Asn72) (Table 2). In some of the peptides, the relative intensities of residues close to the N terminus of the protein were also affected (Table 2). It is interesting to note that the relative intensity of the cross-peak of Thr68 in the presence of any of the peptides did not show a variation larger than 15 %, whereas it has been shown to change during the binding of NUPR1 to small molecules (24). However, the relative intensities of cross-peaks of nearby residues (Glu63, Asn72 and Ser73) were largely affected upon peptide binding (Table 2).

As there were changes only in the intensities of the cross-peaks (and not in their chemical shifts), the equilibrium-exchange between the peptide- free and bound wild-type NUPR1 must be intermediate-to-slow within the NMR time scale. It could be thought that those variations in the spectral intensity were due to a larger solution viscosity (which may be altered by the presence of the peptides) (59); however, at the maximal total biomolecular concentration used in this work (~500 μM), we have not observed broadening in the spectra of isolated NUPR1 (22). In fact, NUPR1 does not aggregate up to concentrations of 2 mM, where its NMR assignment has been carried out (22). In addition, it could be suspected that the pH increased during the experiment (or upon addition of the peptide), resulting in signal-broadening due to solvent-exchange. However, the pH measurements before and after spectra acquisition indicate that the pH remained constant during the experiments (see section 2.6). The fact that signal broadening was only observed upon peptide addition suggests that the binding between NUPR1 and the peptides was responsible for that broadening.

Furthermore, the titration experiments carried out by following the HSQC spectra at different peptide concentrations suggest that the decrease in intensity of the cross-peaks of NUPR1 spectra was peptide-dependent (Fig. S7). This decrease was larger for P-2, in agreement with the larger affinity constant determined by ITC (Table 1), the gold-standard in determining thermodynamic parameters of binding reactions (58). Moreover, the fact that the decrease in intensity does not occur at the same pace for all the residues indicate that the binding was not a two-state process, as it could be inferred from the results in Table 2 at a single peptide concentration: different cross-peaks show several changes in their relative intensities. It could be thought that a K_D could be obtained from the fitting of the decrease in absolute intensities of each of the different cross-peaks for each of the peptides; however, a reliable value for a dissociation constant cannot be obtained from the changes in intensities for intermediate-to-slow exchange rates within the NMR time scale, as it has been widely discussed (60).

In conclusion, the NMR experiments further confirm that there was binding between the peptides and wild-type NUPR1, involving, at least at a first stage, mainly residues around the 30s region of the NUPR1 sequence.

3.4. In silico calculations predicted the regions involved in the peptide binding

A systematic search was performed to study *in silico* the binding of NUPR1 with the peptides. To overcome the computational limitation in treating large numbers of torsional degrees of freedom of IDPs, molecular docking was carried out using seven-residue-long fragments spanning the whole sequence of wild-type NUPR1, and an ensemble of the structures of the peptides as hosts. Although the scoring obtained provides only an empirical approximation of the association affinity, molecular docking has already proved to be effective with NUPR1 to identify binding to other small compounds (24). Furthermore, an accurate determination of the conformational ensemble of the IDP is not a prerequisite for the findings presented below, because docking is applied considering only isolated fragments of the primary structure of NUPR1.

Figure S8 shows the binding scores obtained for the segments of NUPR1, calculated as a function of the protein sequence. The energy differences among the four peptides were comparable with those observed in the docking of the fragments with different structures of the same peptide (~ 0.3 kcal/mol, on average); therefore, all the data for each peptide were combined to increase their statistical significance. The predicted segments of the NUPR1 sequence that contribute the most to the binding correspond to minima in the curve (Fig. S8), and include: the 30s region; the polypeptide patch around Thr54; and the two protein termini (with the lowest values found for Thr8 and Asn72/Ser73, which are close to the N and C terminus, respectively). These regions agree nicely with those observed to experience the larger broadening changes in all peptides by NMR (Table 2, see section 3.3). On the other hand, those values of the theoretical binding energies (Table 1) were slightly less favorable than the experimental ones (-5.5 kcal/mol *versus* -7.2 kcal/mol for P-3). Importantly enough, such predicted regions did not include the polypeptide patch around residue Thr68, which was important for the anchoring of small compounds (24), whereas they still include the other key region of relatively high hydrophobicity around Ala33, which was important for the interaction of NUPR1 with the other binding partners (20,22-24).

Once we had identified the NUPR1 region centered around Ala33 as that contributing most to the binding affinity of the peptides, we sought to use this information to pinpoint the preferred binding region in the latter. To this aim, we mapped the binding poses of the seven-residue fragment centered on Ala33 onto the structure of each of the peptides (Fig. 4). The results clearly indicate that only about half of the helical surface of the peptide was involved in the binding, and this interacting region was common to all of them. Interestingly, the binding patch was on the same side where residue 11 is placed, and regardless whether it is an Arg (as in P-1 and P-3) or a Val residue (P-2 and P-4). More importantly, the binding patch did not overlap with the most hydrophobic region of the helical peptides, suggesting that hydropathy is not the sole determinant of the peptide/NUPR1 association. This binding patch (formed among others by Val1, Trp4, Met5 and Leu9) is the same involved to form the self-associated helical region in the intact capsid protein of HIV-1; thus, the

peptides use the same region to interact with other biomolecules (NUPR1) or with themselves (26). These results support the experimental fluorescence experiments (see section 3.2.), in which the environment around Trp4 in the peptides was affected upon binding to NUPR1.

The findings above are apparently difficult to reconcile with the experimental observation that the Thr68Gln mutant (which disrupts the hydrophobicity pattern in that specific region of the NUPR1 sequence) did not bind to the peptides (Figs. S2 and S3). To investigate this aspect, MD simulations were performed of both wild-type NUPR1 and the Thr68Gln mutant, with peptide P-2, for which the largest changes were observed (Table 2, Fig. 3), placed on the protein surface in correspondence to Ala33. For wild-type NUPR1, we observed a capture mechanism of the peptide (Fig. 5), where P-2 appeared to maintain a stable α-helical conformation at the end of the binding process. The protein had a more compact N-terminal region and an extended C-terminal patch, which possesses a higher amount of positively charged residues. The presence of Thr68 provides a slightly higher hydrophobicity and favors the collapse of the protein C terminus on the helical peptide, allowing the flanking residues Glu63 and Asn72 to approach the ligand surface. Thus, the gradient of hydrophobicity along the NUPR1 sequence plays a crucial role in the binding mechanism, although it is not a main factor in maintaining the anchoring of the peptides.

Although our simulations were performed starting with the hydrodynamic radius of the NUPR1 ensemble close to the experimental value measured by NMR (24, 45) possible artifacts due to overcompaction of an IDP are usually a concern during MD simulations. To exclude a potential influence on the binding mechanism described above, additional control simulations were performed using the TIP4P-D water model (47), which avoids disordered protein ensembles less expanded compared to the experiment. As a result, we observed (Fig. S9) for wild type NUPR1 an interaction with the peptide analogous to the one described in Fig. 5. In particular, Ala33 maintained the binding with the helical peptide while Thr68 favored the approach of the protein C terminus, driving the nearby residues Glu63 and Asn72 towards the ligand surface. Besides being an independent validation under simulation conditions that do not favor the complex formation (because solute-

solvent interactions are increased with the use of the TIP4P-D water model (47)), we point out that this effect does not involve an overcompaction of NUPR1 structure, which would involve a stable interaction of the Thr68 residue with the peptide. In contrast, the mechanism described explains why mutation of Thr68 affects the binding without this residue being listed in a binding patch.

In summary, although the docking procedure could not eventually discriminate among the quantitative differences in the binding of the four peptides (Table 1), it provided an accurate identification of the critical regions for the binding to NUPR1. Furthermore, the MD simulations clarified the molecular details in the peptide association.

3.5. Evidence for the interaction of peptides with NUPR1 within an intracellular environment

To test whether the interaction between the peptides and wild-type NUPR1 occurred within cells and the peptides were capable of inhibiting the binding of NUPR1 with one of its natural partners, we carried out studies *in cellulo*. Our previous results showed that C-RING1B efficiently and specifically interacted with wild-type NUPR1 (23). Subsequently, we sought to detect whether the peptides interacted with NUPR1 and blocked its interaction with C-RING1B by using the Duolink *in situ* assay, which resolves the binding of proteins that occurs at distances lower than 16 Å. We performed controls experiments transfecting a FITC-antibody, as a control peptide included in the kit (Fig. S10), in order to monitor the internalization of the peptides, and the possible effect in the interaction between the two proteins. The control peptide did not change the interaction between the two proteins *in cellulo*.

When interaction between the two proteins takes place, red fluorescent spots appear, corresponding to the positive PLA signal. Our results show that only peptides P-1 and P-3 efficiently interacted with wild-type NUPR1 (Fig. 6) and blocked the interaction between the two proteins, diminishing the red fluorescent spots, corresponding to the PLA signals. Different attempts to replicate this behaviour with P-2 and P-4, by using several transfection times, were always unsuccessful. We believe that the presence of the Arg (and its positive charge) adjacent to the C-terminal residue of the peptides (Table 1) allows cell insertion, as the two peptides with such residue

at this position led to successful PLAs. For the rational design of further peptides inhibiting PPIs of NUPR1, the presence of this residue should be ensured.

Thus, taken together, these results demonstrate that a specific peptide/NUPR1 complex forms within cultured cells. These findings confirm the biological relevance of our simulations and the *in vitro* biophysical and biochemical experiments.

4. DISCUSSION

4.1. Peptides as inhibitors of NUPR1 functions

The importance of the network of interactions between proteins (known as interactome) for understanding the functioning of living organisms and the development of diseases is widely acknowledged (7). Despite this, drugs designed to target PPIs are relatively rare (when compared to other designed small molecules aiming to specific polypeptide binding sites). Moreover, drug design is particularly challenging when some of the macromolecules involved in the PPIs are IDPs. NUPR1 exerts several functions by specific interactions with other biomolecules (DNA or proteins). We have recently found a small drug, TFP, capable of binding to NUPR1 and inhibiting its functions, thus mimicking the cellular effects observed in the absence of this protein (24). However, the hot-spot region of NUPR1 is a discontinuous epitope (8) involving two distant polypeptide patches: (i) that at the 30s in the NUPR1 sequence; and, (ii) a region close to Thr68 and the C terminus. TFP shows a proximity to both Ala33 and Thr68 in the NMR experiments and in MD simulations of the complex (24). Mutations at those key positions (Ala33 and Thr68) have resulted in impaired NUPR1 mutants where binding to its natural partners is severely decreased (23).

We and others have designed small molecules against IDPs capable of interfering with their PPIs or nucleic-acid interactions (24, 61-68), and there are a few examples in the literature where peptides are used as inhibitors of PPIs involving IDPs (69-71), or several approaches for folded proteins (see 2 and references therein). In these examples, the peptides are designed based on either similarity with the sequence of the partner protein or, alternatively, fitting with the disordered region(s) of the IDP. In all of them, the protein (or protein region involved in the binding) remained basically disordered, with changes in the conformational ensemble of the protein (64). Furthermore, several α-helix peptidomimetics have also been designed based on the α-helix scaffold of the original protein sequence that the IDP binds to (72). In NUPR1, we have not designed peptides based on the sequence of one of its partners neither on any homologous sequence to NUPR1, but rather we have carried out hypothesis-driven experiments by exploiting physico-chemical principles based on

the amphipathy and helicity of a series of peptides with a natural tendency to adopt helical structures. There were poor linear relationships between each of these isolated properties and the values of the measured K_D (Table 1) with linear regression coefficients no larger than 60 %. Thus, it is the interplay of both physico-chemical properties, helicity and amphipathy, which seems to allow the specific binding to NUPR1, and not a single property. However, since we have a rough estimation of the percentage of α-helix- or turn-like structures from the CD measurements, we cannot rule out other factors determining the K_D values, such as the entropic contribution due to the solvent or the shape of the peptides, with their corresponding structured conformation.

4.2. Molecular basis of peptide/NUPR1 complex formation

We experimentally observed that the assayed peptides bound *in vitro* to NUPR1 (Table 2, Figs. 3 and S6) at the same regions involved in binding to other biomolecules: the 30s region and the neighbourhood of Thr68. In fact, the region around Thr68 was critical for the binding of the peptides, since experiments with the Thr68Gln mutant did not yield any binding (Figs. S2, S3). This residue did not contribute energetically very much to the binding (as suggested by the simulation, Figs. 4 and S8), but it was critical in directing the binding mechanism (Fig. 5). Therefore, we can conclude that NUPR1 uses the same discontinuous epitopes (or "short lineal motifs", SLiMs), which facilitate multivalent interactions with other molecules (73) to bind to any partner. Some SLiMs in other IDPs have also been shown to function as high promiscuous binders: for instance, the transactivation domain of p53 interacts with multiple proteins, by using the same motif with structurally distinct binding modes upon engagement with its several partners (74). In the case of the peptides, other SLiMs of NUPR1 (together with the regions around Thr68 and Ala33) appeared to be involved in the binding, probably due to the larger size of the peptides compared to that of small drugs (24).

Upon binding to the peptides, NUPR1 remained disordered, as judged by the absence of changes in chemical shifts in most of the cross-peaks in the NMR spectra (Fig. 3 and Fig. S6), and the lack of sigmoidal behaviour in the thermal denaturations measured by CD (Fig. S5) and fluorescence. The cross-peaks of residues, that became broadened, might indicate that the

corresponding amino acids are involved in other conformations where they could form more local structured regions, but these local structures must not be very rigid due to the lack of sigmoidal transitions in thermal denaturations. In the particular case of P-2, since most of the signals became broadened and disappeared (Fig. 3), we could not rule out the presence of more structured conformations, although they cannot be very stable due to: (i) the features of the thermal denaturation curves of the complexes; and, (ii) the absence of large changes in the CD spectrum of the complex when compared to that of isolated NUPR1 (as it happens with P-3, Fig. S5). The fact that the cross-peaks of different residues became broadened before those of other amino acids (Fig. S7, Table 2) suggests also that the binding is not a two-state process, and it must involve several populations of peptides with helix-like conformations, or, alternatively NUPR1 conformations with several local residual structure. We suggest that peptide binding must involve a change of NUPR1 conformational ensemble from a random set in the isolated protein to a particular subset of conformers (and that is why only a subset of cross-peaks were broadened in each peptide). This shift must require a reduction in the entropy of the whole system (peptide and protein) caused by steric, hydrophobic or electrostatic effects. The persistently disordered conformation of NUPR1 seems to be a general feature (20, 22-24): whatever molecule (synthetic small molecule, DNA, protein and peptide) binds to the IDP, it is not capable of altering its disordered nature. Furthermore, in all these molecules, the binding equilibrium seems to have an intermediate-to-slow exchange rate within the NMR time-scale (22-24, 60).

At this stage, we do not know the structure acquired by the peptides upon binding to NUPR1, but from MD simulations, the structure seems to be α-helical (Figs. 4, 5). The helical propensity of the peptide was decreased in the control runs performed with the TIP4P-D water model (Fig. S9), but it is not clear whether this is a cost of increasing the solute-solvent dispersion interactions that improve the disorder propensity in the IDP (47). Furthermore, based on two pieces of evidence, we believe that the helical structure acquired by the peptides upon binding, as suggested by the MD simulations, is weak. First, we did not observe sigmoidal, co-operative thermal denaturations

monitored by CD or fluorescence for the complexes (Fig. 1C, Fig. S5 B). And second, the binding of NUPR1 to the peptides is not a two-state process as concluded from the different decrease regimes in NMR cross-peaks intensities for several residues (Fig. S7); it is likely that the peptides, upon binding to NUPR1, shift the equilibrium towards more populated helical conformations, but all of those helical conformations are capable, to a larger or lesser extent, of binding to NUPR1. Finally, it is important to note that the peptides interacted with NUPR1 through residues located in the proximity of Trp4 (Fig. S4), as it has been observed when these peptides are bound to other proteins or in their own self-association (26); thus, peptides also employ the same (hydrophobic) residues to interact with different molecules.

4.3. Energetic and thermodynamic determinants of the peptide/NUPR1 interaction

The measured K_D of NUPR1 for interacting with the peptides (Table 1) was similar to that observed for MSL1 (~3 μM) (22), for prothymosin α (~6 μM) (20), C-RING1B (~12 μM) (23) and for different drugs capable of inhibiting the binding between NUPR1 and MSL1 (~5 μM) (24). Such affinity is relatively small, but it allows a proper regulation of the several pathways where NUPR1 is involved (18), achieving a high specificity despite a moderate binding energy. Moderate affinities (i.e., in the range 1-10 μM) are not rare for other IDPs, and they have been measured during the formation of "fuzzy" complexes, where the partners remain disordered after complex formation (75, 76); these fuzzy complexes facilitate fast binding since no disorder-to-order transition is happening. Thus, binding between both molecules goes beyond the classical archetypes of conformational selection or induced fit since both are sampling a range of conformations continuously.

It is important to note that our peptides self-associate in solution (with a self-association constant of ~4 μM) (26); therefore, peptide binding to NUPR1 would be coupled to peptide dissociation, and the apparent dissociation constant (K_D, Table 1) for the peptide/NUPR1 complex will contain an energetic penalty associated with the peptide dissociation event. Thus, the intrinsic dissociation constant for the peptide/NUPR1 interaction would be lower (i.e. more favorable binding

affinity, see section 3.2.). The effect of the peptide self-association has not been considered quantitatively and explicitly in the interaction experiments (fluorescence and ITC). For that, we would need to know the peptide self-dissociation constant (in the range of ~4 μM, as measured by CD titrations (26)) and the self-dissociation enthalpy. However, from the measured apparent dissociation constant for the peptide/NUPR1 interaction (Table 1), we can state that the intrinsic dissociation constant for the peptide/NUPR1 interaction would be somewhat smaller. Other biomolecules interacting with NUPR1 are either monomeric (prothymosin α (20)) or oligomeric (C-RING1B (23) and MSL1 (22)), although in the MSL1 case, we do not know its exact self-association state.

4.4. Perspectives in the design of helical peptides for inhibition of IDPs

Although there are several FDA approved peptides for therapeutic use (77) and the future holds promising for others to be approved (78), in general, the current therapeutic application of peptides is limited due to low cell penetration and marked propensity to proteolysis and metabolic degradation. We observed some of these features in our design: only peptides P-1 and P-3 were able to hamper the interaction of C-RING1B and NUPR1 *in cellulo*. Although we cannot rule out the cytotoxicity of peptides P-2 and P-4, we suggest that cell-permeation was facilitated in P-1 and P-3 by the presence of an Arg residue at the second-to-last position in peptide sequence (Table 1). An alternative explanation could be that this residue provides critical electrostatic interactions in a surface patch that is key for binding to the 30s region of NUPR1, as pointed out by our docking results. In either case, future designs of the peptides will probably require a positive charge at this position of the sequence. At this stage, it is tempting to speculate that P-1 and P-3 might be even particularly effective in conjunction with TFP to prevent PPIs of NUPR1.

Furthermore, our studies suggest that helicity was not the sole factor governing peptide affinity of the peptides, since there was not a clear relationship between the helicity experimentally measured (or the value theoretically calculated) and the measured affinities (Table 1). Although we cannot rule

out that peptide self-association could mask a clear relationship between those physico-chemical parameters, it seems that there are other additional factors governing the peptide binding to NUPR1. In fact, our *in silico* results pinpoint a specific peptide region (that marked in Fig. 4) that may be improved through a rational design, to modulate the binding to NUPR1. However, a delicate balance in the sequence should be maintained to preserve the amphipathic properties of the peptides, since the presence of a hydrophobic patch on their surface appears to be equally important to drive the binding of the C-terminal region of NUPR1.

5. CONCLUSIONS

Our results represent a proof-of-concept for the use of peptides with tuned physico-chemical properties to bind an IDP, and without any homology of sequence with respect to the target IDP. Furthermore, they show that peptides can be effectively used *in cellulo* as inhibitors of PPIs essential for IDPs biological functions. These findings open the possibility to use designed peptides (or peptidomimetics) as regulators of these challenging "druggable-targets".

AUTHOR CONTRIBUTIONS AND COMPETING INTERESTS

PSC, JLI, OA, AVC, BR and JLN designed the experiments and the research methodology. PSC, AVC, OA, BR and JLN carried out the experiments and analyzed data. PSC, JLI, BR, AVC, OA and JLN wrote the paper. The authors declare no competing interests.

ACKNOWLEDGEMENTS

The authors thank the two reviewers for helpful suggestions and discussion. This work was supported by Spanish Ministry of Economy and Competitiveness [CTQ 2015-64445-R (to JLN), BFU2013-47064-P and BFU2016-78232-P (to AVC)]; by the French La Ligue Contre le Cancer, INCa, Canceropole PACA, DGOS (labellisation SIRIC) and INSERM (to JLI) and Fundación Alfonso Martín-Escudero (to PSC). The Spanish Fondo de Investigaciones Sanitarias [PI15/00663 (to OA)]; Spanish Miguel Servet Program from Instituto de Salud Carlos III [CPII13/0017 (to OA)]; regional Diputacion General de Aragon “Digestive Pathology Group B01” (to OA) and “Protein Targets Group B89” (to AVC); Centro de Investigacion Biomedica en Red en Enfermedades

Hepáticas y Digestivas (CIBERehd); and Asociacion Española de Gastroenterologia (AEG). BR acknowledges kind hospitality in the Magnetic Resonance Center (CERM), Sesto Fiorentino (Florence), Italy.

SUPPLEMENTARY INFORMATION

There are ten figures describing: the interaction of P-1, P-2 and P-4 with wild-type NUPR1 followed by ANS fluorescence (Fig. S1); the interaction of P-3 with Thr68Gln mutant by fluorescence (Fig. S2) and ITC (Fig. S3); the fluorescence titrations of P-1 and P-4 (Fig. S4); the interaction of wild-type NUPR1 with P-3 monitored by CD (Fig. S5); the 2D ^{1}H, ^{15}N-HSQC NMR spectra of NUPR1 when P-1, P-3 and P-4 are added (Fig. S6); the decrease in absolute intensity for selected residues measured in the HSQC cross-peaks for the four peptides (Fig. S7), as their concentration was increased; the energetic results obtained by molecular docking (Fig. S8); the capture mechanism of a helical peptide by NUPR1 in simulation under conditions favouring a relatively less compacted protein state (Fig. S9); and the control experiment with the test peptide kit for the *in cellulo* experiments (Fig. S10).

REFERENCES

1. Fischer, G., Rossmann, M., and Hyvönen, M. (2015) Alternative modulation of protein-protein interactions by small molecules. *Curr. Opin. Biotechnol*. **10**, 78-85.

2. Cunningham, A. D., Qvit, N., and Mochly-Rosen, D. (2017) Peptides and peptidomimetics as regulators of protein-protein interactions. *Curr. Opin. Struct*. *Biol.* **44**, 59-66.

3. London, N. Raveh, B., Movshovitz-Atthias, D., and Schueler-Furman, O. (2010) Can self-inhibitory peptides be derived from the interfaces of globular protein-protein interactions? *Proteins* **78**, 3140-3149.

4. Bullock, B. N., Jochim, A. L., and Aurora, P. S. (2011) Assessing helical protein interfaces for inhibitor design. *J. Am. Chem. Soc*. **133**, 14220-14223.

5. Berman, H. M., Westbrook, J., Feng, Z., Gilliland, G., Bhat, T. N., Weising, H., Shindyalov, I. N., and Bourne, P. E. (2000) The protein data bank. *Nucl. Acids Res*. **28**, 235-242.

6. Smith, M. C., and Gestwicki, J. E. (2012) Features of protein-protein interactions that translate into potent inhibitors: topology, surface area and affinity**.** *Expert. Rev. Mol. Med.* **14**: e16.

7. Arkin, M. R., Tang, Y., and Wells, J. A. (2014) Small-molecule inhibitors of protein-protein interactions: progressing towards the reality. *Chem. Biol*. **21**, 1102-1114.

8. Scott, D. E., Bayley, A. R., Abell, C., and Skidmore, J. (2016) Small molecules, big targets: drug discovery faces the protein-protein interaction challenge. *Nat. Rev. Drug Discov*. **15**, 533-550.

9. London, N., Raveh, B., and Schueler-Furman, O. (2013) Druggable protein-protein interactions-from hot spots to hot segments. *Curr. Opin. Chem. Biol*. **17**, 952-959.

10. Pelay-Gimeno, M., Glas, A., Koch, O., and Grossmann, T.N. (2015) Structure-based design of inhibitors of protein-protein interactions: mimicking peptide binding epitopes. *Angew. Chem. Int. Ed*. **54**, 8896-8927.

11. Frackenpohl, J., Ardvisson, P. I., Schreiber, J. V., and Seebach, D. (2001) The outstanding biological stability of beta- and gamma-peptides toward proteolytic enzymes: an *in vitro* investigation with fifteen peptidases. *ChemBiochem* **2**, 445-455.

12. Wiegand, H., Wirz, B., Schweitzer, A., Camenisch, G. P., Rodríguez-Pérez, M. I., Gross, G., Woessner, R., Voges, R., Arvidsson, P. I., Frackenpohl, J., and Seebach, D. (2002) The outstanding metabolic stability of a ^{14}C-labeled beta-nonapeptide in rats-*in vitro* and *in vivo* pharmacokinetic studies. *Biopharm. Drug Dispos.* **23**, 251-262.

13. Mallo, G.V., Fiedler, F., Calvo, E.L., Ortiz, E.M., Vasseur, S., Keim, V., Morisset, J., and Iovanna, J.L. (1997) Cloning and expression of the rat p8 cDNA, a new gene activated in pancreas during the acute phase of pancreatitis, pancreatic development, and regeneration, and which promotes cellular growth. *J. Biol. Chem.* **272**, 32360-32369.

14. Uversky, V.N. (2013) A decade and a half of protein intrinsic disorder: biology still waits for physics. *Protein Sci.* **22**, 693-724.

15. Tompa, P. (2012) Intrinsically disordered proteins: a 10-year recap. *Trends Biochem. Sci.* **37**, 509-516.

16. Wright, P.E., and Dyson, H.J. (2015) Intrinsically disordered proteins in cellular signalling and regulation. *Nat. Mol. Cell Biol.* **16**, 18-29.

17. Cano, C.E., Hamidi, T., Sandi, M.J., and Iovanna, J.L. (2011) Nupr-1: the Swiss knife of cancer *J. Cell Physiol.* **226**, 1439-1443.

18. Goruppi, S., and Iovanna, J.L. (2010) Stress-inducible protein p8 is involved in several physiological and pathological processes. *J. Biol. Chem.* **285**, 1577-1581.

19. Hamidi, T., Algül, H., Cano, C.E., Sandi, M.J., Molejon, M.I., Riemann, M., Calvo, E.L., Lomberk, G., Dagorn, J.C., Weih, F., Urrutia, R., Schmid, R.M., and Iovanna, J.L. (2012) Nuclear

protein 1 promotes pancreatic cancer development and protects cells from stress by inhibiting apoptosis. *J. Clin. Invest.* **122**, 2092-2103.

20. Malicet, C., Giroux, V., Vasseur, S., Dagorn, J.C., Neira, J.L., and Iovanna, J.L. (2006) Regulation of apoptosis by the p8/prothymosin alpha complex. *Proc. Natl. Acad. Sci. USA* **103**, 2671-2676.

21. Encinar, J.A., Mallo, G.V., Mizyrycki, C., Giono, L., González-Ros, J.M., Rico, M., Cánepa, E., Moreno, S., Neira, J.L., and Iovanna**,** J.L. (2001) Human p8 is a HMG-I/Y-like protein with DNA binding activity enhanced by phosphorylation. *J. Biol. Chem.* **276**, 2742-2751.

22. Aguado-Llera, D., Hamidi, T., Doménech, R., Pantoja-Uceda, D., Gironella, M., Santoro, J., Velázquez-Campoy, A., Neira, J.L., and Iovanna**,** J.L. (2013) Deciphering the binding between Nupr1 and MSL1 and their DNA-repairing activity. *PLoS One* **8**, e78101.

23. Santofimia-Castaño, P., Rizzuti, B., Pey, A. L., Soubeyran, P., Vidal, M., Urrutia, R., Iovanna J. L., and Neira, J.L. (2017) Intrinsically disordered chromatin protein NUPR1 binds to the C-terminal region of Polycomb RING1B. *Proc. Natl. Acad. Sci. USA* **114**: doi: 10.1073/pnas.1619932114.

24. Neira, J.L., Bintz, J., Arruebo, M., Rizzuti, B., Bonacci, T., Vega, S., Lanas, A., Velázquez-Campoy, A., Iovanna**,** J.L., and Abián, O. (2017) Identification of a drug targeting an intrinsically disordered protein involved in pancreatic adenocarcinoma. *Sci. Reports* **7**, 39732.

25. Díaz-Gómer, J. L., Castorena-Torres, F., Preciado-Ortiz, R. E., and García Lara, S (2017) Anti-cancer activity of maize bioactive peptides. *Front. Chem.* **5**, 44.

26. Doménech, R., Bocanegra, R., González-Muñiz, R., Gómez, J., Mateu, M. G., and Neira, J. L. (2011) Larger helical populations in peptides derived from the dimerization helix of the capsid protein of HIV-1 results in peptide binding toward regions other than the "hotspot" interface. *Biomacromolecules* **12**, 3252-3264.

27. Muñoz, V., and Serrano, L. (1994) Elucidating the folding problem of helical peptides using empirical parameters. *Nat. Struct. Biol*. **1**, 399-409.

28. Lacroix, E., Viguera, A.R., and Serrano, L. (1998) Elucidating the folding problem of alpha-helices: local motifs, long-range electrostatics, ionic-strength dependence and prediction of NMR parameters. *J. Mol. Biol*. **284**, 173-191.

29. Miroux, B., and Walker, J.E. (1996) Over-production of proteins in *Escherichia coli*: mutant hosts that allow synthesis of some membrane proteins and globular proteins at high levels. *J. Mol. Biol.* **260**, 289-288.

30. Gill, S.C., and von Hippel, P.H. (1989) Calculation of protein extinction coefficients from amino acid sequence data. *Anal. Biochem*. **182**, 319-326.

31. Ganser-Pornillos, B.K., Yeager, M., and Sundquist, W. (2008) The structural biology of HIV assembly. *Curr. Opin. Struct. Biol*. **18**, 203-217.

32. Mateu, M.G. (2009) The capsid protein of human immunodeficiency virus: intersubunit interactions during virus assembly. *FEBS J.* **276**, 6098-6109.

33. Beckett, D. (2011) Measurement and analysis of equilibrium binding titrations: a beginner's guide. *Methods Enzymol*. **488**, 1–16.

34. Royer, C.A., and Scarlatta, S. F. (2008) Fluorescence approaches to quantifying biomolecular interactions. *Methods Enzymol*. **450**, 79–106.

35. Birdsall, B., King, R. W., Wheeler, M. R., Lewis, C. A. Jr., Goode, S., Dunlap, R. B., and Roberts, G. C. (1983). Correction for light absorption in fluorescence studies of protein-ligand interactions. *Anal. Biochem*. **132**, 353–361.

36. Cavanagh, J.F., Wayne, J., Palmer III, A.G., and Skelton, N.J. (1996) *Protein NMR spectroscopy: principles and practice*. Academic Press, San Diego, California.

37. Bodenhausen, G., and Ruben, D. (1980) Natural abundance nitrogen-15 NMR by enhanced heteronuclear spectroscopy. *Chem. Phys. Lett*. **69**, 185-189.

38. Marcus, D., Hanwell, M.D., Curtis, D.E., Lonie, D.C., Vandermeersch, T., Zurek, E., and Hutchison, G.R. (2012) Avogadro: An advanced semantic chemical editor, visualization, and analysis platform. *J. Cheminform*. **4**, 17.

39. Humphrey,W., Dalke, A., and Schulten, K. (1996) VMD: visual molecular dynamics. *J. Mol. Graph. Model.* **14**, 33-8-27-8.

40. Hess, B., Kutzner, C., van der Spoel, D., and Lindahl, E. (2008) GROMACS 4: Algorithms for highly efficient, load-balanced, and scalable molecular simulation. *J. Chem. Theory Comp*. **4**, 435-447.

41. Lindorff-Larsen, K., Piana, S., Palmo, K., Maragakis, P., Klepeis, J.L., Dror, R.O., and Shaw, D.E. (2010) Improved side-chain torsion potentials for the Amber ff99SB protein force field. *Proteins* **78**, 1950-1958.

42. Jorgensen, W.L., Chandrasekhar, J., Madura, J.D., Impey, R.W., and Klein, M.L. (1983) Comparison of simple potential functions for simulating liquid water. *J. Chem. Phys.* **79**, 926-935.

43. Guzzi, R., Rizzuti, B., and Bartucci, R. (2012) Dynamics and binding affinity of spin-labeled stearic acids in beta-lactoglobulin: evidences from EPR spectroscopy and molecular dynamics simulation. *J. Phys. Chem. B* **116**, 11608-11615.

44. Pantusa, M., Bartucci, R., and Rizzuti, B. (2014) Stability of trans-resveratrol associated with transport proteins. *J. Agric. Food Chem*. **62**, 4384-4391.

45. Neira, J.L., Rizzuti, B., and Iovanna, J.L. (2016) Determinants of the pK_a values of ionizable residues in an intrinsically disordered protein. *Arch. Biochem. Biophys.* **598**, 18-27.

46. Cozza, C., Neira, J.L., Florencio, F.J., Muro-Pastor, M.I., and Rizzuti, B. (2017) Intrinsically disordered inhibitor of glutamine synthetase is a functional protein with random-coil-like pK_a values. *Protein Sci*. **26**, 1105-1115.

47. Piana, S., Donchev, A. G, Robustelli, P., Shaw, D. E. (2015) Water dispersion interactions strongly influence simulated structural properties of disordered protein states. *J. Phys. Chem. B* **119**, 5113-5123.

48. Abascal, J. L. F., and Vega, C. (2005) A general purpose model for the condensed phases of water: TIP4P/2005. *J. Chem. Phys*. **123**, 234505–1-12.

49. Morris. G.M. (2009) AutoDock4 and AutoDockTools4: automated docking with selective receptor flexibility. *J. Comp. Chem.* **30**, 2785-2791.

50. Trott, O., and Olson, A.J. (2010) Software news and update AutoDock Vina: improving the speed and accuracy of docking with a new scoring function, efficient optimization, and multithreading. *J. Comp. Chem*. **31**, 455-461.

51. Fraga, H., Papaleo, E., Vega, S., Velázquez-Campoy, A., and Ventura, S. (2013) Zinc induced folding is essential for TIM15 activity as an mtHsp70 chaperone. *Biochim. Biophys. Acta* **1830**, 2139-2149.

52. Kanuru, M., Samuel, J.J., Balivada, L.M., and Aradhyam, G.K. (2009). Ion-binding properties of Calnuc, Ca^{2+} versus Mg^{2+}--Calnuc adopts additional and unusual Ca^{2+}-binding sites upon interaction with G-protein. *FEBS J*. **276**, 2529-2546.

53. Uversky, V.N., Gillespie, J.R., Millett, I.S., Khodyakova, A.V., Vasilenko, R.N., Vasiliev, A.M., Rodionov, I.L., Kozlovskaya, G.D., Dolgikh, D.A., Fink, A.L., Doniach, S., Permyakov, E.A. and Abramov, V.M. (2000) Zn(2+)-mediated structure formation and compaction of the "natively unfolded" human prothymosin α. *Biochem. Biophys. Res. Commun.* **267**, 663-668.

54. Abian, O., Vega, S., Sancho, J., and Velázquez-Campoy, A. (2013) Allosteric inhibitors of the NS3 protease from the hepatitis C virus. *PloS One* **8**, e69773.

55. Abian, O., Vega, S., Neira, J. L., and Velázquez-Campoy, A. (2010) Conformational stability of hepatitis C virus NS3 protease. *Biophys. J.* **99**, 3811-3820.

56. Abian, O., Neira, J. L. and Velázquez-Campoy, A. (2009) Thermodynamics of zinc binding to hepatitis C virus NS3 protease: A folding by binding event. *Proteins* **77**, 624-636.

57. Holdgate, G. A., Anderson, M., Edfeldt, F., and Geschwindner, S. (2010) Affinity-based, biophysical methods to detect and analyze ligand binding to recombinant proteins: matching high information content with high throughput. *J. Struct. Biol*. **172**, 142-157.

58. Linkuviene, V., Kariner, G., Chen, W.Y., and Matulis, D. (2016) Isothermal titration calorimetry for drug design: precision of the enthalpy and binding constant measurements and comparison of the instruments. *Anal. Biochem.* **515**, 61-64.

59. Pastore, A., and Temussi, P.A. (2017) The Emperor's new clothes: myths and truths of in-cell NMR. *Arch. Biochem. Biophys.* **628**, 114-122.

60. Teilum, K., Kunze, M. B., Erlendsson, S., and Kragelun, B. B. (2017) (S)Pinning down protein interactions by NMR. *Protein Sci*. **26**, 436-451.

61. Toth, G., Garadia, S.J., Zago, W., Beronicin, C.W., Cremades, N., Roy, S.L., Tambe, M.A., Rochet, J.C., Galvagnion, C., Skibinski, G., Finkbeiner, S., Bova, M., Regnstrom, K., Chiou, S.S., Johnston, J., Callaway, K., Anderson, J.P., Jobling, M.F., Buell, A.K., Yednock, T.A., Knowles, T.P., Vendruscolo, M., Christodoulou, J., Dobson, C.M., Schenk, D., and McConlogue, L. (2014) Targeting the intrinsically disordered structural ensemble of α-synuclein by small molecules as a potential therapeutic strategy for Parkinson disease. *PLoS One* **9**, e87133.

62. Iconaru, L. I., Ban, D., Bharatham, K., Ramanathan, A., Zhang, W., Shelat, A.A., Zuo, J., and Kriwacki, R.W. (2015) Discovery of small molecules that inhibit the disordered protein, p27(Kip1). *Sci. Rep*. **5**, 15686.

63. Ban, D., Iconaru, L.I., Ramanathan, A., Zuo, J., and Kriwacki, R.W. (2017) A small molecule causes a population shift in the conformational landscape of an intrinsically disordered protein. *J. Am. Chem. Soc.* **139**,13692-13700.

64. Krishnan, N., Koveal, D., Miller, D.H., Xue, B., Akshinthala, S.D., Kragelj, J., Jensen, M.R., Gauss, C.M., Page, R., Blackledge, M., Muthuswamy, S. K., Peti, W., and Tonks, N.K. (2014) Targeting the disordered C terminus of PTP1B with an allosteric inhibitor. *Nat. Chem. Biol.* **10**, 558-566.

65. Erkizan, H V., Kong, Y., Merchant, M., Schlottmann, S., Barber-Rotenberg, J.S., Yuan, L., Abaan, O.D., Chou, T.H., Dakshanamurthy, S., Brown, M.L., Metallo, S.J., Üren, A., and Toretsky, J.A. (2009) A small molecule blocking oncogenic protein EWS-FLI1 interaction with RNAS helicase A inhibits growth of Erwing's sarcoma. *Nat. Medicine* **15**, 750-757.

66. Follis, A. V., Hammoudeth, D. I., Wang, H., Prochwonik, E. V., and Metallo, S. J.(2008) Structural rationale for the coupled binding and unfolding of the c-Myc oncoprotein by small molecules. *Chem. Biol.* **15**, 1149-1155.

67. Fletcher, S., and Prochwonik, E. V. (2015) Small molecule inhibitors of the Myc concoprotein. *Biochim. Biophys. Acta* **1849**, 525-543.

68. Zhang, Y., Appleton, B. A., Wiesman, C., Lau, T., Costa, M., Hannoush, R. N., and Sidhu, S. (2009) Inhibition of Wnt signalling by dishevelled PDZ peptides. *Nat. Chem. Biol.* **5**, 217-219.

69. Hammoudeth, D. I., Follis, A. V., Prochwonik, E. V., and Metallo, S. J. (2009) Multiple binding sites for small-molecule inhibitors on the oncoprotein c-Myc. *J. Am. Chem. Soc.* **131**, 7390-7401.

70. Metallo, S.J. (2010) Intrinsically disordered proteins are potential drug targets. *Cur. Opin. Chem. Biol.* **14**, 481-488.

71. Jung, K.-Y., Wang, H., Teriete, P., Yap, J. L., Chen, L., Lanning, M.E., Hu, A., Lambert, L. J., Holien, T., Sundan, A., Cosford, N.D., Prochownik, E.V., and Fletcher, S. (2015) Perturbation of the c-Myc-Max protein-protein interaction via synthetic α-helix mimetics. *J. Med. Chem*. **58**, 3002-3024.

72. Mittag, T., Orlicky, S., Choy, W.Y., Tang, X., Lin, H., Sicheri, F., Kay**,** L.E., Tyers, M., and Forman-Kay**,** J.D. (2008) Dynamic equilibrium engagement of a polyvalent ligand with a single-site receptor. *Proc. Natl. Acad. Sci. USA* **105**, 17772-17777.

73. Berlow, R.B., Dyson, H.J., and Wright, P.E. (2015) Functional advantages of dynamic protein disorder. *FEBS Lett.* **589**, 2433-2440.

74. Khan, H. Cino, E.A., Brickenden, A., Fan, J., Yang, D., and Choy, W.Y. (2013) Fuzzy complex formation between the intrinsically disordered prothymosin α and the kelch domain of Keap1 involved in the oxidative stress response. *J. Mol. Biol.* **425**, 1011-1027.

75. Miskei, M., Antal, C., and Fuxreiter, M. (2017) FuzDB: database of Fuzzy complexes, a tool to develop stochastic structure-function relationships for protein complexes and higher-order assemblies. *Nucl. Acids Res.* **45**, D228-D235.

76. Hyde, E. I., Callow, P., Rajsekar, K. V., Timmins, P., Patel, T. R., Siligardi, G., Hussain, R., White, S. A., Thomas, C. M., and Scott, D. J. (2017) Intrinsic disorder in the partitioning protein KorB persists after co-operative complex formation with operator DNA and KorA. *Biochem. J.* **474**, 3121-3135.

77. Usmani, S. S., Bedi, G., Samuel, J. S., Singh, S., Kalra, S., Kumar, P., Ahuja, A. A., Sharma, M., Gautam, A., and Raghava, G. P. S. (2017) THPdb: Database of FDA-approved peptide and protein therapeutics. *PLoS One* **12**, e0181748.

78. Fosgerau, K., and Hoffmann, T. (2015) Peptide therapeutics: current status and future directions? *Drug Discov. Today* **20**, 122-128.

Table 1: Sequences, percentage of helical structure and thermodynamic parameters in the NUPR1 binding of the peptides [a].

Peptide	% of helical structure (AGADIR)[b]	% of helical structure (from CD measurements) [b]	K_a (M^{-1})[c]	K_D (μM)[c]	ΔH (kcal mol^{-1})[c]	K_D (μM)[d]
Ac-VKNWMTETLLRQ-NH_2 (P-1)	13.90	8.4	9.4×10^5	1.1	1.3	2.3 ± 0.8
Ac-VKNWMTEYLLVQ-NH_2 (P-2)	24.80	5.7	1.8×10^6	0.57	1.7	1.6 ± 0.7
Ac-VKNWMTEYLLRQ-NH_2 (P-3)	52.88	8.2	3.1×10^5	3.2	1.2	2 ± 1
Ac-VKNWMTETLLVQ-NH_2 (P-4)	4.59	6.9	4.4×10^5	2.2	1.5	0.4 ± 0.2

[a]The P-4 is the wild-type sequence. Errors in the calorimetric measurements are estimated to be 15-20 % for K_a and K_D and 5% for ΔH.

[b]Data from (26).

[c]Determined from ITC measurements. Measurements were carried out at 15 ºC.

[d]Determined from fluorescence titrations. Errors are fitting errors to Eq. 1. Measurements were carried out at 25 ºC.

Table 2: Resonances of NUPR1 residues, whose relative intensities (with respect to Arg82) were affected by the presence of the peptide [a]

Peptide	Resonances[b]
Ac-VKNWMTETLLRQ-NH_2 (385 μM) (P-1)	Thr8 (+); Glu18; Ala33 (+); Gly39; Gly44; Ala50 (+); Glu63; Asn72; Ser73
Ac-VKNWMTEYLLVQ-NH_2 (385 μM)[c] (P-2)	All cross-peaks broadened
Ac-VKNWMTEYLLRQ-NH_2 (405 μM) (P-3)	Thr3; Thr8 (+); Glu18; Gly39; Gly44; Ala50; Thr54; Glu63; Asn72
Ac-VKNWMTETLLVQ-NH_2 (230 μM) (P-4)	Thr8 (+); Glu18; Ala33 (+); Gly39; Gly44; Glu63; Asn72

[a]Only residues whose signals could be unambiguously integrated (that is, non-overlapping cross-peaks) are indicated. The peptide concentration used is indicated within parenthesis beside each peptide sequence. NUPR1 concentration was 190μM. Experiments were carried out at pH 4.5 and 25 ºC.

[b]Residues with "+" sign indicate that the intensity variation was ~45 % of the relative intensity of the same cross-peak in the spectrum of the isolated NUPR1. Residues that showed variations in the relative intensity of cross-peaks (when compared to that in isolated NUPR1) larger than 15 % are indicated.

[c]P-2 was also tested at 430 μM concentration.

FIGURE LEGENDS

FIGURE 1: **Intrinsic and ANS-fluorescence characterization of the binding between P-3 and wild-type NUPR1**: (A) Fluorescence spectrum after excitation at 370 nm, in the presence of ANS, of the complex P-3/NUPR1 (15: 20 μM) and that obtained by the addition of the spectra of each isolated molecule. (B) Fluorescence spectrum, after excitation at 280 nm, of the complex P-3/NUPR1 and that obtained by the addition of the spectra of each isolated molecule. (C) Fluorescence thermal denaturations followed by the emission at 480 nm, after excitation at 370 nm (in the presence of ANS) of the isolated NUPR1 (green, blank circles), P-3 (blue line) and of the complex (black line).

FIGURE 2: **ITC of wild-type NUPR1 and the peptides**: Calorimetric titrations for (from left to right): P-1, P-2, P-3 and P-4. Thermograms (top) and binding isotherms (bottom) are shown. Non-linear fittings according to a model considering a single ligand binding site (continuous lines) are shown for each peptide.

FIGURE 3: **Interaction of wild-type NUPR1 and P-2 mapped by 2D ^{1}H, ^{15}N-HSQC spectra**: Overlay of wild-type NUPR1 spectra at 0 (black); and 385 (red) μM (in protomer units) of P-2. The same low contour level was used for both spectra. Experiments were acquired at pH 4.5 and 25 ºC.

FIGURE 4: **Preferred binding poses of the seven-residue-long NUPR1 sequence fragment centered on Ala33 onto the peptides**. Binding modes calculated by using the AutoDock Vina (50) docking engine for the protein segment 30-36 of NUPR1 are mapped onto the ideal helical structure of the peptides (superimposed by rototranslation on the C^{α} atoms, and represented as a solid tube with the position of amino acids 1-7 shown as transparent volumes). The wheel scheme corresponding to an ideal α-helix is

also displayed on the left, with the region showing the highest hydrophobicity indicated with a black line on top.

FIGURE 5: **Capture mechanism of an α-helical peptide by NUPR1**. The protein is oriented with the more compact N-terminal region at the bottom and the extended C-terminal region on top, with selected residues labeled. The P-2 peptide (in orange) is shown using a surface representation of the backbone.

FIGURE 6: ***In situ* PLA of peptides and wild-type NUPR1**. Mouse anti-HA and rabbit anti-human wild-type NUPR1 were used to reveal the interaction between the C-RING1B and NUPR1 in HeLa cells. PLA was carried out as described (22,23) after cells were treated with the peptides (170 μM) for 4 h.

Figure 1

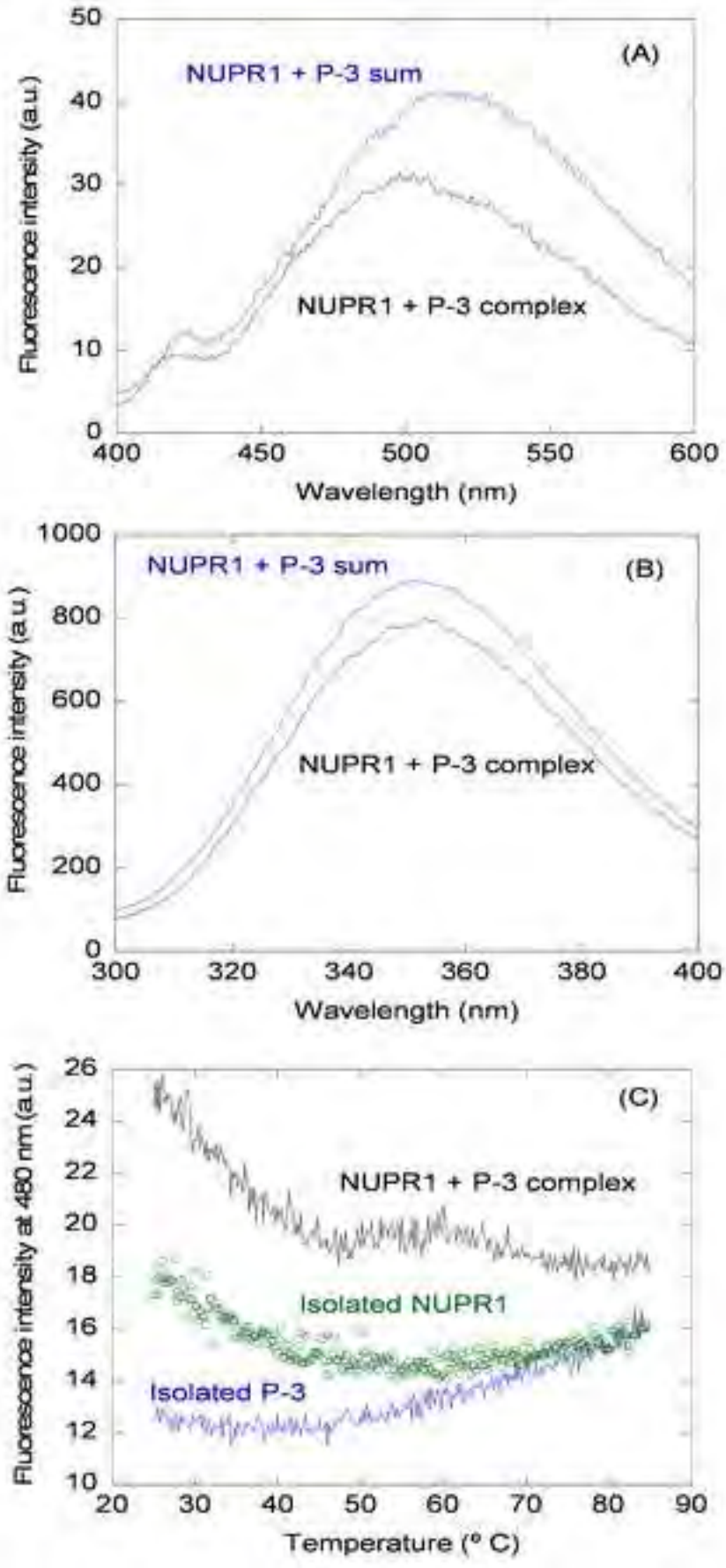
(A)
NUPR1 + P-3 sum
NUPR1 + P-3 complex
Fluorescence intensity (a.u.)
Wavelength (nm)
(B)
NUPR1 + P-3 sum
NUPR1 + P-3 complex
Fluorescence intensity (a.u.)
Wavelength (nm)
(C)
NUPR1 + P-3 complex
Isolated NUPR1
Isolated P-3
Fluorescence intensity at 480 nm (a.u.)
Temperature (° C)

Figure 2

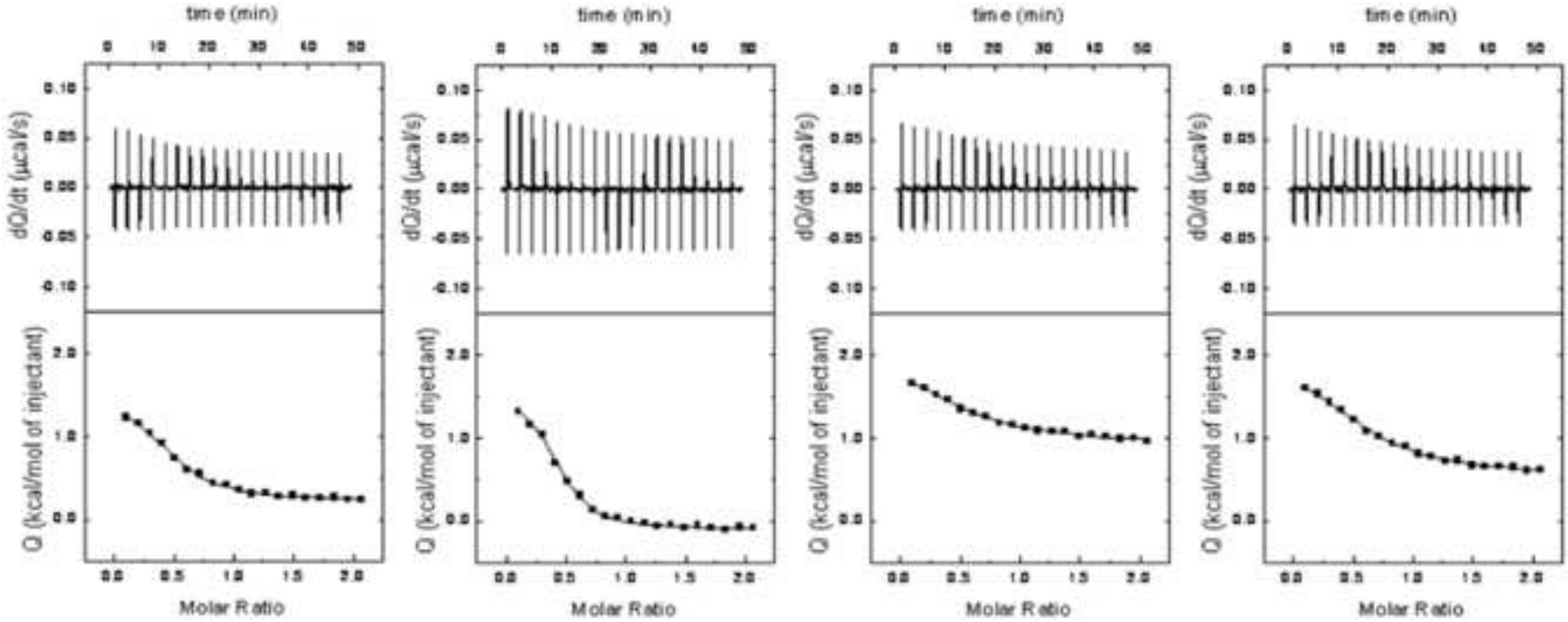

Figure 3

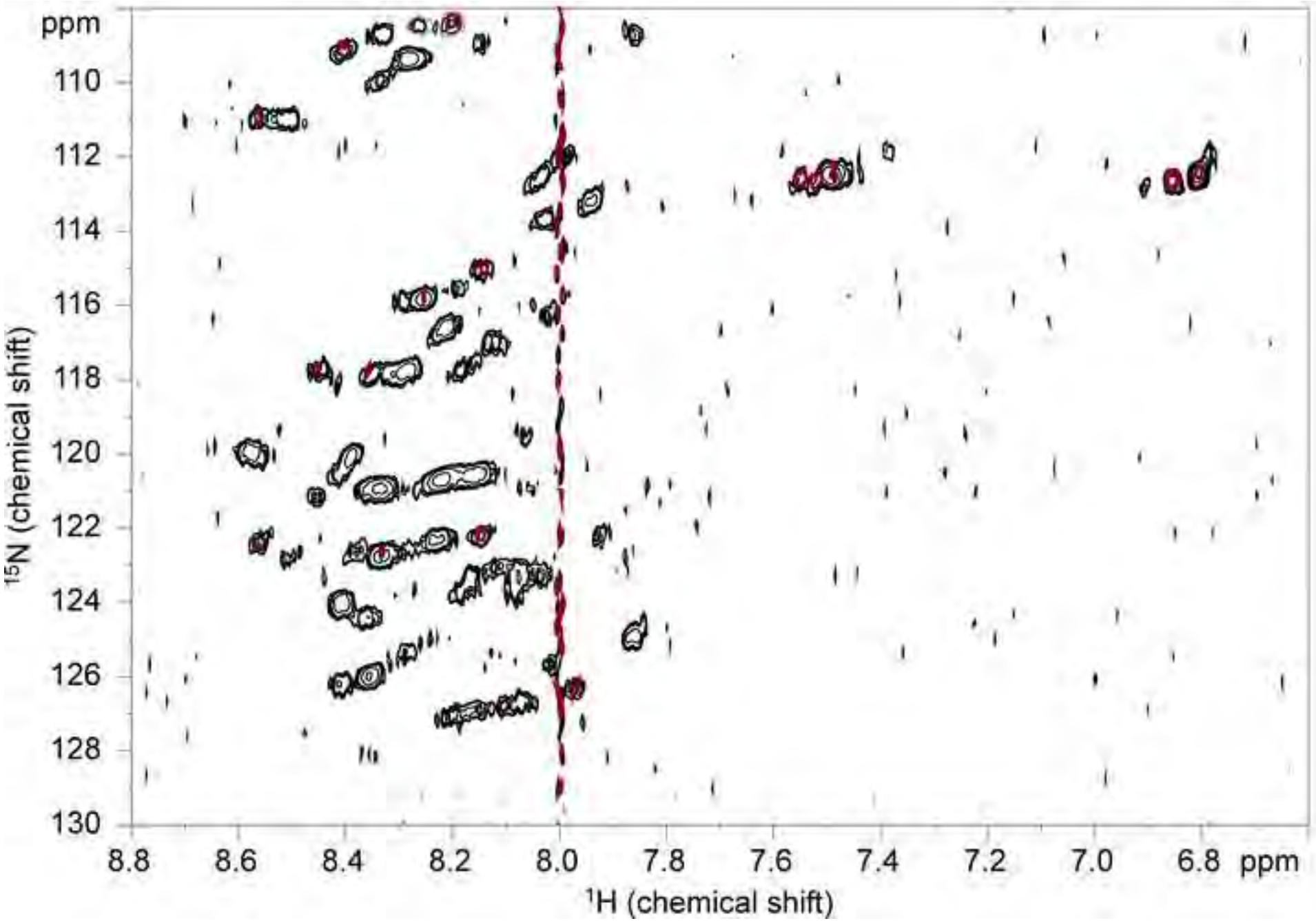
ppm
110
112
114
116
118
120
122
124
126
128
130
15N (chemical shift)
8.8
8.6
8.4
8.2
8.0
7.8
7.6
7.4
7.2
7.0
6.8 ppm
1H (chemical shift)

Figure 4

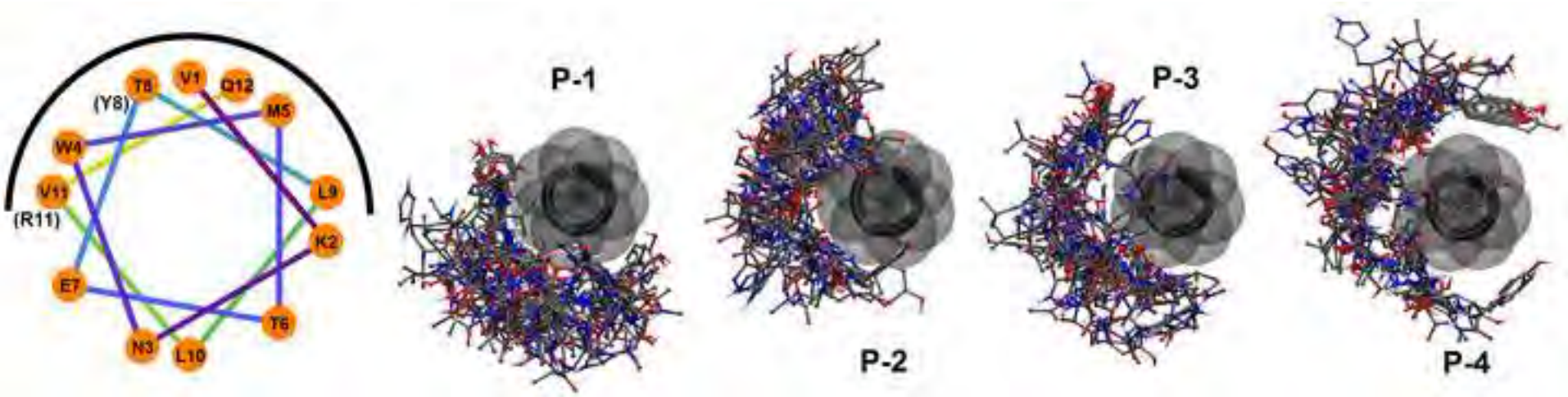

Figure 5

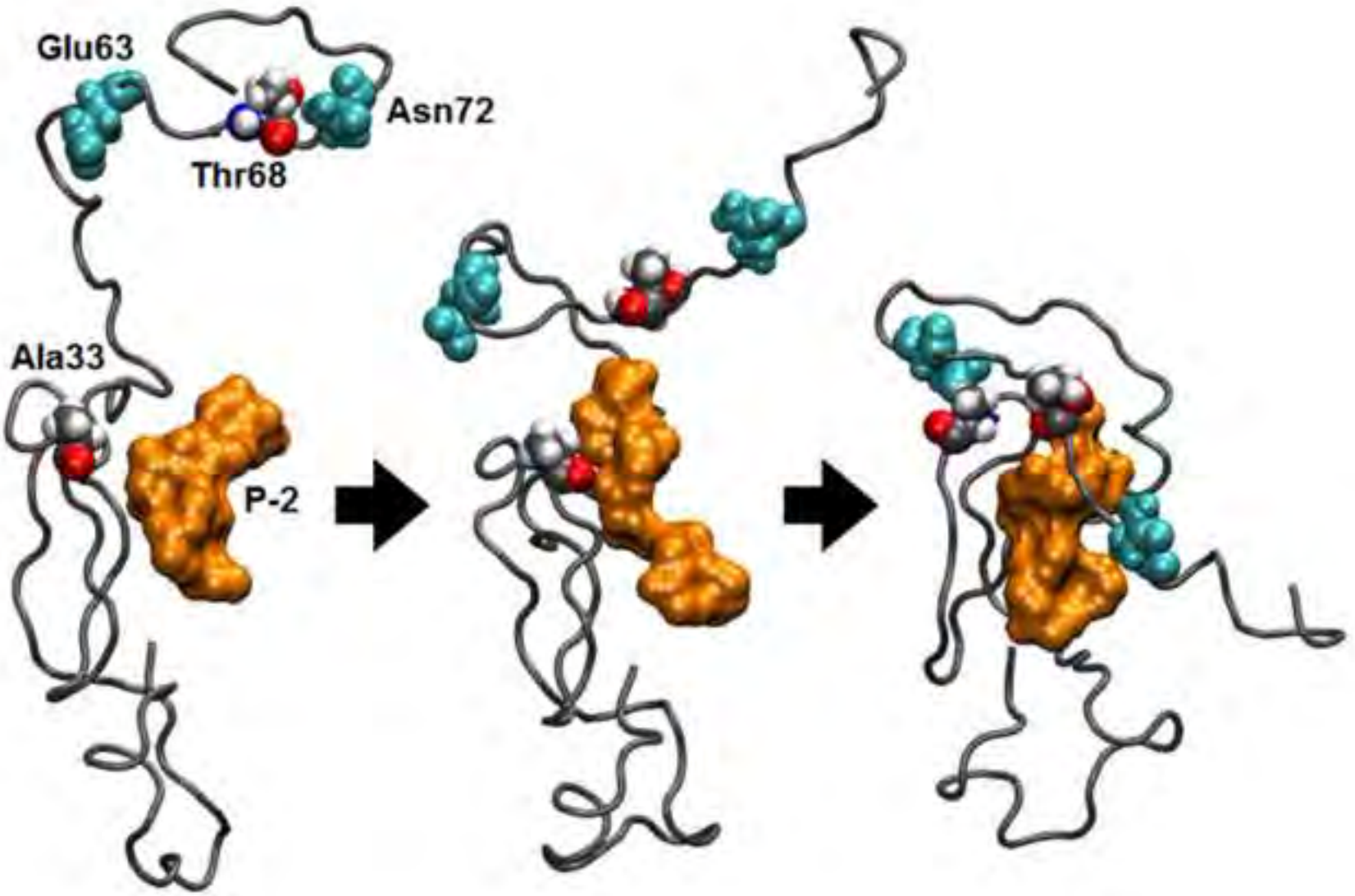

Figure 6

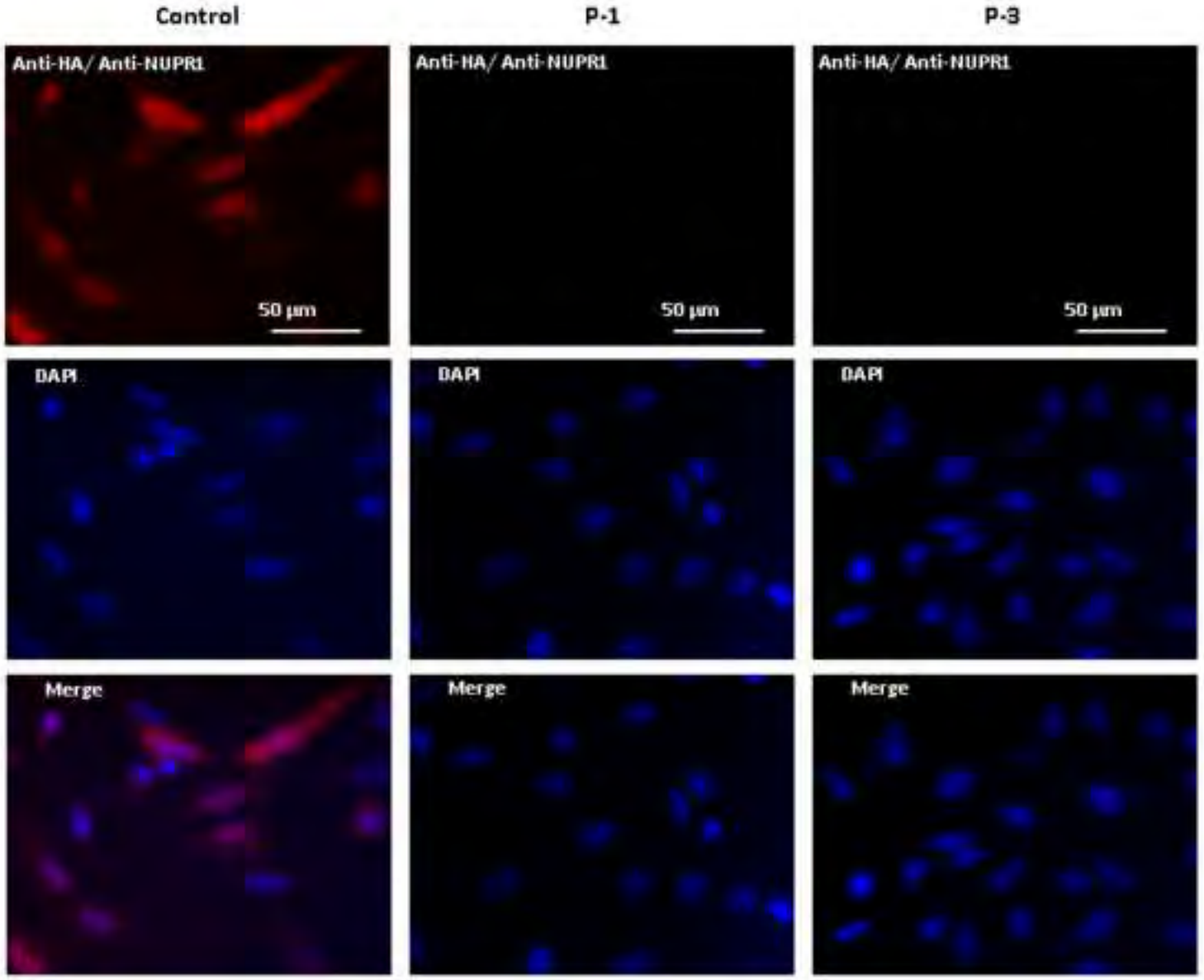

S10 (Santofimia-Castaño et al.)

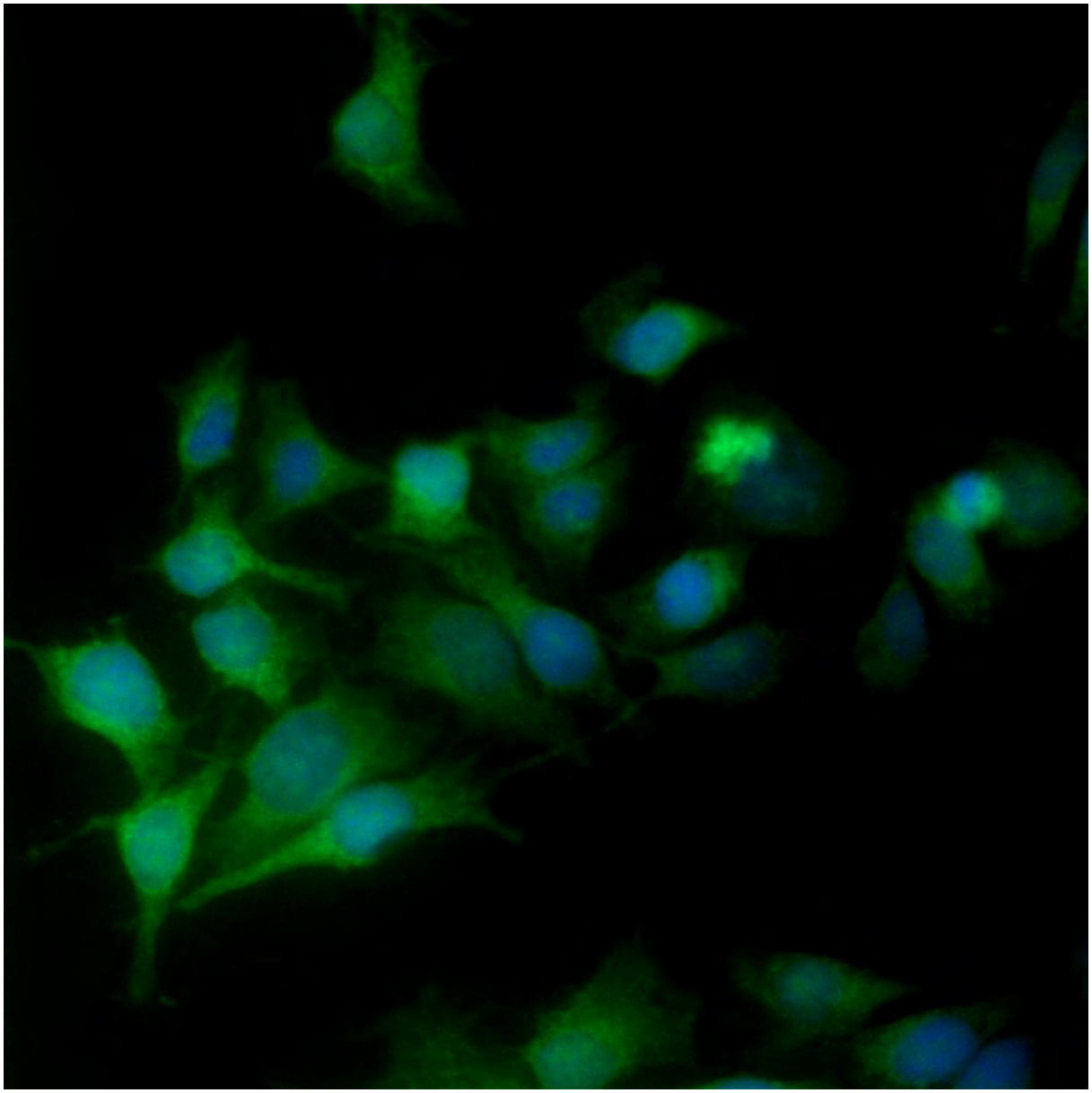

***Conflict of Interest form**

Click here to download Conflict of Interest form: Interestpeptides.doc